AFRL-RV-PS-TR-2018-0110

AFRL-RV-PS-TR-2018-0110

EXTENSIONS TO PREDICTIVE CONTROL AND PARAMETER GOVERNORS FOR APPLICATIONS TO AUTONOMOUS VEHICLES AND VEHICLE FORMATIONS

Ilya Kolmanovsky and Anouck Girard

Regents of the University of Michigan
Office of Research and Sponsored Projects
503 Thompson Street
Ann Arbor, MI 48109-1340

23 November 2018

Final Report

APPROVED FOR PUBLIC RELEASE; DISTRIBUTION IS UNLIMITED.

AIR FORCE RESEARCH LABORATORY
Space Vehicles Directorate
3550 Aberdeen Ave SE
AIR FORCE MATERIEL COMMAND
KIRTLAND AIR FORCE BASE, NM 87117-5776

DTIC COPY

NOTICE AND SIGNATURE PAGE

Using Government drawings, specifications, or other data included in this document for any purpose other than Government procurement does not in any way obligate the U.S. Government. The fact that the Government formulated or supplied the drawings, specifications, or other data does not license the holder or any other person or corporation; or convey any rights or permission to manufacture, use, or sell any patented invention that may relate to them.

This report is the result of contracted fundamental research which is exempt from public affairs security and policy review in accordance with AFI 61-201, paragraph 2.3.5.1. This report is available to the general public, including foreign nationals. Copies may be obtained from the Defense Technical Information Center (DTIC) (http://www.dtic.mil).

AFRL-RV-PS-TR-2018-0110 HAS BEEN REVIEWED AND IS APPROVED FOR PUBLICATION IN ACCORDANCE WITH ASSIGNED DISTRIBUTION STATEMENT.

//signed//

CHRISTOPHER PETERSEN
Program Manager

//signed//

DAVID WILT
Tech Advisor, Spacecraft Component Technology Branch

//signed//

JOHN BEAUCHEMIN
Chief Engineer, Spacecraft Technology Division
Space Vehicles Directorate

This report is published in the interest of scientific and technical information exchange, and its publication does not constitute the Government's approval or disapproval of its ideas or findings.

REPORT DOCUMENTATION PAGE

Form Approved
OMB No. 0704-0188

1. REPORT DATE *(DD-MM-YYYY)*	**2. REPORT TYPE**	**3. DATES COVERED** *(From - To)*
23-11-2018	Final Report	26 May 16 – 23 Nov 18

4. TITLE AND SUBTITLE
Extensions to Predictive Control and Parameter Governors for Applications to Autonomous Vehicles and Vehicle Formations

5a. CONTRACT NUMBER

5b. GRANT NUMBER
FA9453-16-1-0069

5c. PROGRAM ELEMENT NUMBER
62601F

6. AUTHOR(S)
Ilya Kolmanovsky and Anouck Girard

5d. PROJECT NUMBER
8809

5e. TASK NUMBER
PPM00023423

5f. WORK UNIT NUMBER
EF127615

7. PERFORMING ORGANIZATION NAME(S) AND ADDRESS(ES)
AND ADDRESS(ES)
Regents of the University of Michigan
Office of Research and Sponsored Projects
503 Thompson Street
Ann Arbor, MI 48109-1340

8. PERFORMING ORGANIZATION REPORT NUMBER

9. SPONSORING / MONITORING AGENCY NAME(S) AND ADDRESS(ES)
Air Force Research Laboratory
Space Vehicles Directorate
3550 Aberdeen Ave., SE
Kirtland AFB, NM 87117-5776

10. SPONSOR/MONITOR'S ACRONYM(S)
AFRL/RVSV

11. SPONSOR/MONITOR'S REPORT NUMBER(S)
AFRL-RV-PS-TR-2018-0110

12. DISTRIBUTION / AVAILABILITY STATEMENT
Approved for public release; distribution is unlimited.

13. SUPPLEMENTARY NOTES

14. ABSTRACT
Novel Model Predictive Control algorithms and design procedures were developed for waypoint following by autonomous vehicles, while accommodating dynamically changing prediction horizon. Novel algorithms and design procedures also were developed for parameter governors to safely maneuver multi-vehicle formations to desired configurations while satisfying pointwise-in-time state and control constraints. The developed predictive control strategies have demonstrated in simulation scenarios representing spacecraft and spacecraft formations missions and maneuvers.

15. SUBJECT TERMS
Model Predictive Control, MPC, Robust Decentralized Model Predictive Control, RDMPC, Approximate Dynamic Programming, ADP, Hybrid Projected Gradient-Evolutionary Search Algorithm, HPGES, Multi-Agent, Real Time

16. SECURITY CLASSIFICATION OF:			**17. LIMITATION OF ABSTRACT**	**18. NUMBER OF PAGES**	**19a. NAME OF RESPONSIBLE PERSON**
a. REPORT	**b. ABSTRACT**	**c. THIS PAGE**			Christopher Petersen
Unclassified	Unclassified	Unclassified	SAR	48	**19b. TELEPHONE NUMBER** *(include area code)*

Standard Form 298 (Rev. 8-98)
Prescribed by ANSI Std. 239.18

(This page intentionally left blank)

TABLE OF CONTENTS

LIST OF FIGURES

Figure **Page**

ACKNOWLEDGEMENTS AND DISCLAIMER

Acknowledgement
This material is based on research sponsored by Air Force Research Laboratory under agreement number FA9453-16-1-0069. The U.S. Government is authorized to reproduce and distribute reprints for Governmental purposes notwithstanding any copyright notation thereon.

(This page intentionally left blank)

1. SUMMARY

The focus of the research was to expand the capabilities of predictive controllers, including parameter governors, Nonlinear Model Predictive Controllers (NMPC) and waypoint following controllers, and to demonstrate the potential for the use of these extensions in spacecraft control problems as prototypical autonomous vehicle related control problems.

Specific progress has been made in the following areas:

1. Developing invariance-based methods for constrained relative motion planning and control which connect waypoints corresponding to Natural Motion Trajectories (NMTs) that may correspond to equilibria or periodic/non-periodic time-varying unforced trajectories,
2. Establishing an NMPC controller for constrained spacecraft attitude control including waypoint following, and demonstrating the implementation of this controller on a 3-degree-of-freedom air bearing spacecraft motion simulator,
3. Expanding the capabilities of the parameter governor solutions for generating and maintaining autonomous networked spacecraft formations subject to state and control constraints,
4. Developing models for spacecraft information collection, and control methods for use in constrained satellite inspection missions.
5. Developing a Model Predictive Control (MPC) algorithm for waypoint following in the presence of constraints while minimizing the computational footprint, for use in concert with a dynamically changing prediction.

The following publications have been published, written, or are in the process of being written, and are related to the subject matter of this report:

- Frey, G., Petersen, C., Leve, F, Kolmanovsky, I., and Girard, A., “Constrained spacecraft relative motion planning exploiting periodic natural motion trajectories and invariance,” AIAA Journal of Guidance, Control, and Dynamics, Vol. 40, No. 12, AIAA, 2017, pp. 3100-3115.

- Frey, G., Petersen, C., Leve, F., Kolmanovsky, I., and Girard, A., “Incorporating periodic and non-periodic natural motion trajectories into constrained invariance-based spacecraft relative motion planning,” Proceedings of 1st IEEE Conference on Control Technology and Applications (CCTA), Kohala Coast, HI, 2017, pp. 1811-1816.
- Frey, G., Petersen, C., Leve, F., Garone, E., Kolmanovsky, I., and Girard, A., “Parameter governors for coordinated control of -spacecraft formations,” AIAA Journal of Guidance, Control, and Dynamics, Vol. 40, No. 11, AIAA, 2017, pp. 3020-3025.
- Frey, G., Petersen, C., Leve, F., Girard, A., and Kolmanovsky, I., “Safe relative motion trajectory planning for satellite inspection.” Proceedings of AAS/AIAA Space Flight Mechanics Meeting, No. 7-411, AAS/AIAA, San Antonio, TX, 2017.

- Frey, G., “Advances in constrained spacecraft relative motion planning,” *Ph.D. Dissertation,* The University of Michigan, 2018.
- Liao-McPherson, D., Dunham, W., and Nicotra, M., “Plant model and optimal control problem for spacecraft NMPC,” Notes, 2018.
- Sutherland, R., Kolmanovsky, I., Girard, A., Leve, F., Petersen, C., “Minimum-time model predictive spacecraft attitude control for waypoint following and exclusion zone avoidance”, *2019 AIAA SciTech Forum*, AIAA, San Diego, CA, January 2019 (accepted, to appear)
- Sutherland, R., Kolmanovsky, I., Girard, A., “Waypoint following MPC in minimum time”, *Notes, 2018.*

2. INTRODUCTION

Two key considerations in the design of control schemes for autonomous vehicles in general, and for spacecraft in particular, are computational load and constraint enforcement. Spacecraft frequently have strict volume, mass, and power limitations which limit on-board computing capabilities. Additionally, constraints such as control actuation limits and obstacle or exclusion zone avoidance must be satisfied to ensure safe operations. Because these constraints may be non-linear and non-convex, their presence complicates the application of standard optimization and control methods.

Several broad classes of control techniques have been shown to be effective in enforcing these types of constraints. Model Predictive Control (MPC) techniques [1, 2], in which a model of the dynamics is used to predict system behavior over a time horizon. System inputs are selected to optimize a cost function subject to constraints, have been previously applied to spacecraft control problems, see, e.g., [3-8]. Reference Governors and Command Governors [9] which modify the reference provided to a nominal closed-loop system controller in order to satisfy constraints, and Parameter Governors [10], which modify parameters in the closed loop system to the same end, have also been shown to be effective solutions for constrained spacecraft control, e.g., [11-14]. Finally, predictive control methods based on set invariance and chained invariant/contractive sets have been developed [15, 16], including a method developed by Principal Investigor PI Kolmanovsky and his collaborators to generate safe trajectories via a graph search through a set of waypoints corresponding to forced equilibria in a relative motion frame [17].

One potential mission application for spacecraft control, and specifically spacecraft relative motion planning, is satellite inspection. In this application, one or more spacecraft are used to gather information (imagery, radio signals, etc.) about another spacecraft. Several current programs, including Defense Advanced Research Projects Agency DARPAs Robotic Servicing of Geosynchronous Vehicles (RSGS) [18] and the Air Force’s Geosynchronous Space Situational Awareness Program [19] illustrate the utility of satellite inspection missions. Previous work for these types of missions has focused on design requirements for inspector spacecraft [20, 21] or on trajectory design considering specific figures of merit such as image resolution or fuel expenditure [22].

In this report, we summarize our work in developing several novel predictive spacecraft control methods which can be used to generate constraint-satisfying trajectories (either rotational or translational), and in developing models and trajectory generation methods to be used in the specific application of satellite inspection.

3. METHODS, ASSUMPTIONS, AND PROCEDURES

3.1 Invariance-Based Constrained Spacecraft Relative Motion Control

In this section, a novel predictive approach to spacecraft relative motion control with obstacle avoidance and thrust saturation constraints is described. This approach is based on a graph search applied to a "virtual net" of Natural Motion Trajectories (NMTs), to determine a sequence of waypoints, representing NMTs, which are used to generate a safe trajectory between specified starting and ending NMTs. In the virtual net, the NMTs represent virtual net nodes and adjacency and connection information is determined by conditions defined in terms of safe, positively invariant tubes built around each trajectory. These conditions guarantee that transitions from one NMT to another NMT can be completed without constraint violations. This newly developed approach improves the flexibility of a previous approach developed by the PI and his collaborators [17], and has other advantages in terms of reduced fuel consumption and passive safety.

3.1.1 Assumptions.

The spacecraft dynamics, relative to a nominal point on a circular orbit, are given by the linear time-invariant Clohessy-Wiltshire (CW) equations [23], which, in discrete-time are

$$X(k+1) = AX(k) + Bu(k), \tag{1}$$

where k designates the discrete-time instants, $X(k)$ is the state vector with components corresponding to relative position and velocity, and $u(k) = K\big(X(k) - X_n(k+\delta)\big)$ is the control vector corresponding to continuous thrust forces. In the control law $u(k)$, $X_n(k+\delta)$ is the controller reference along an NMT and K is a gain matrix chosen such that the matrix $A + BK$ is Schur. The discrete-time update period ΔT is chosen to be an integer fraction of the nominal orbital period, τ. The state error is defined as $e(k) = X(k) - X_n(k+\delta)$, and the error dynamics are given by

$$e(k+1) = (A + BK)e(k). \tag{2}$$

A natural motion trajectory $\mathcal{N}$, starting from initial condition X_0 is defined as a finite set of state vectors,

$$\mathcal{N}(X_0) = \mathcal{N} = \{X_n(k) \mid X_n(0) = X_0, \quad X(k+1) = AX_n(k), \quad k \in [0, k_{max}]\}, \tag{3}$$

where $k_{max} = \frac{\tau}{\Delta T}$ for closed (periodic) NMTs and k_{max} is selected for open (non-periodic) NMTs such that the portion of the NMT for $k \in [0, k_{max}]$ lies within the region of interest for the mission. Two constraints are considered. Firstly, the thrust is limited as

$$\|u(k)\|_\infty - u_{max} \leq 0, \quad (4)$$

and secondly, the spacecraft is required to stay out of one or more exclusion zones, modeled as ellipsoidal sets centered at specified points $s_i \in \mathbb{R}^3$ and defined as

$$\mathcal{O}_i(s_i, S_i) = \{X \in \mathbb{R}^6 \mid (\Phi X - s_i)^T S_i (\Phi X - s_i) \leq 1\}, \quad (5)$$

where $S_i = S_i^T > 0$ is a shape matrix and $\Phi = [I_{3\times3} \; 0_{3\times3}]$.

3.1.2 Methods.

Safe, positively invariant tubes are constructed around each NMT in the virtual net. In this context, safe implies that constraints are satisfied point-wise within the tube and "positively invariant" implies that if the spacecraft state is within the tube at a given time instant, and the spacecraft motion is governed by the closed loop dynamics described above, then it will remain within the tube for all future time instants for closed NMTs, or, until the controller reference point is set to $X_n(k_{max})$ for open NMTs. These tubes are formed by first generating safe ellipsoidal sets about each state vector along a NMT, and then adjusting the sizes of these sets such that the tube formed by their union is safe and positively invariant.

An ellipsoidal set, centered at state vector $X_n(k) \in \mathcal{N}$, with scale factor $\rho_k \geq 0$, is defined as

$$\mathcal{E}_{k,\mathcal{N}} = \{X \in \mathbb{R}^6 \mid (X - X_n(k))^T P (X - X_n(k)) \leq \rho_k\}, \quad (6)$$

where the shape matrix $P = P^T > 0$ is chosen to satisfy the discrete Lyapunov inequality. The set $\mathcal{E}_{k,\mathcal{N}}^s$, defined similarly with $\rho_k = \rho_k^s$, is safe if the safe scale factor ρ_k^s is set to the largest possible value such that both the control constraint and the exclusion zone constraints are satisfied point-wise within the set. Safe scale factor calculations, based on the methods developed in [17], are described in [24].

After safe scale factors ρ_k^s have been determined for each state vector $X_n(k) \in \mathcal{N}$, new scale factors, ρ_k, are calculated by making adjustments to ρ_k^s via Procedures 1 or 2 in [24] such that the tube defined by

$$\mathcal{T}_{\mathcal{N}} = \bigcup_{k \in [0, k_{max}]} \mathcal{E}_{k,\mathcal{N}} \quad (7)$$

is both safe, and positively invariant. These procedures are based on the following theorems which give conditions on the scale factors which ensure positive-invariance.

Theorem 1 (Theorem 1 in [24])**:** The tube $\mathcal{T}_{\mathcal{N}}$ is positively-invariant if $\rho_{k_1} \leq \rho_{k_2}$ whenever $k_1 \leq k_2$.

Theorem 2 (Theorem 2 in [24])**:** The tube $\mathcal{T}_{\mathcal{N}}$ is positively-invariant if and only if

$$\rho_k \leq \rho_{k+1} + d(\rho_{k+1}) \ \ \forall \ k \in \mathbb{Z}_{\geq 0}, \tag{8}$$

where

$$\begin{aligned} d(\rho_{k+1}) = \min_{e(k+1)} & \ e(k)^T P e(k) - e(k+1)^T P e(k+1) \\ \text{subject to} & \ \ e(k+1)^T P e(k+1) = \rho_{k+1} \end{aligned} \tag{9}$$

After safe, positively invariant tubes have been constructed for a prescribed set of NMTs, a virtual net is formed. This virtual net consists of a directed graph, with one node corresponding to each closed NMT and one node corresponding to each state vector along each open NMT. The virtual net is represented by an adjacency matrix and connection array, described below. Two nodes are adjacent if it is possible to execute a transfer from the first node to the second while satisfying constraints. Adjacency between nodes is determined using the safe, positively-invariant tubes for each NMT. These adjacency calculations are detailed in [24] for a virtual net composed of only closed NMTs, and in [25] for a virtual net which contains both open and closed NMTs.

The adjacency matrix stores information corresponding to the adjacency of each pair of nodes in the virtual net, and is weighted with an estimate of the control required to execute a safe transfer between adjacent nodes. The connection array stores information needed to perform a fuel-efficient transfer between nodes. Specifically, for each pair of adjacent nodes, the connection array stores the discrete-time indices of the transfer point along the initial NMT and the initial controller reference point along the final NMT that can be used to execute the most fuel-efficient transfer.

Using the adjacency matrix and connection array, fuel-efficient trajectories connecting desired initial and final NMTs are generated. Firstly, Dijkstra's algorithm [26] is applied to the adjacency matrix to obtain a sequence of nodes (waypoints) that can be used to connect the initial and final NMTs. Secondly, the trajectory is generated by switching the controller set point to the next node in the sequence when the spacecraft state enters a small region centered on the transfer point specified in the connection array.

3.2 NMPC for Spacecraft Control

Our research into Nonlinear Model Predictive Control (NMPC) for spacecraft applications has led to the development of a controller for a 3-degree-of-freedom air bearing system subject to nonlinear convex constraints on both state and control variables. This air bearing system is a spacecraft attitude control testbed. We plan on demonstrating attitude waypoint following maneuvers and constrained de-spin maneuvers using this spacecraft attitude control application as a prototypical case study. Computational enhancements are also under the investigation in this setting.

This section summarizes the development of this NMPC spacecraft controller.

3.2.1 Assumptions.

We consider a rigid spacecraft, actuated by three orthogonal thrusters. The orientation of the spacecraft is parametrized by 3-2-1 Euler angles. It is assumed that the attitude representation does not approach singularity; this is consistent with the limitations of the target physical testbed.

The equations of motion are given by

$$
\begin{gathered}
I\dot{w} + w^{\times} I w = u + d\,, \\
\dot{\theta} = S(\theta) w
\end{gathered}
\tag{10}
$$

where w is the vector of angular velocities, θ are the Euler angles, $S(\theta)$ is the inverse kinematic matrix, I is the moment of inertia matrix in a body-fixed frame, u are the control torques and d are unknown, possibly state dependent, disturbances. Collected into a compact form, the model is written as

$$
\dot{x} = f_c(x, u, d), \tag{11}
$$

where $x = [w^T \ \theta^T]^T$.

The prediction model for NMPC is a discretized approximation of the continuous time model (using the Forward Euler integrator and zero order hold assumption) and is given by

$$
x_{k+1} = x_k + \ t_s f_c(x_k, u_k, 0), \tag{12}
$$

where t_s is the discretization time step. The discrete-time prediction model is referred to as

$$
x_{k+1} = f(x_k, u_k). \tag{13}
$$

Note that since the disturbances are unknown, they cannot be incorporated into the prediction model and are assumed to be zero. At time $t = kt_s$, the state estimate is denoted by $x_0 = \hat{x}(t)$.

3.2.2 Methods.

The NMPC optimal control problem (OCP) to be solved for the control to be applied, $u(t) = u_0$ has the following form,

$$
\begin{gathered}
\min_{z} \quad e_i^T Q_f e_i + \sum_{i=0}^{N-1} \left|\left|e_i\right|\right|_Q^2 + \left|\left|u_i\right|\right|_R^2 + s_{i+1} \\
s.t. \;\; x_{i+1} = f(x_i, u_i) + x_i - f(x_{i-1}, u_{i-1}), \qquad i = 0 \dots N-1, \\
c(x_i) \le s_i, \qquad i = 1 \dots N, \\
p(u_i) \le 0, \qquad i = 0 \dots N-1, \\
s_i \ge 0, \qquad i = 1 \dots N
\end{gathered}
\tag{14}
$$

where $e_i = x_i - r$ is the deviation from the target, $z = [u_0^T\ x_1^T\ u_1^T \dots x_N^T]^T$ is the primal optimization variable, N is the length of the prediction horizon, $P = P^T \succcurlyeq 0$ is the terminal penalty, $Q = Q^T \succcurlyeq 0$ is the state penalty weight, $R = R^T \succ 0$ is the control penalty weight, and c, p are the stage state and control constraints respectively.

Note that the state constraints are softened using slack variables in order to ensure the problem is always feasible. The prediction model is written in rate-based form and will automatically compensate for low frequency unmodeled disturbances.

To solve the above OCP, we first write it in compact form as

$$\begin{aligned} \min_{z} \quad & F(z, \xi), \\ s.t. \quad & g(z, \xi) = 0, \\ & c(z) \leq 0, \end{aligned} \tag{15}$$

and introduce the Lagrangian,

$$L(z, \lambda, v, \xi) = F(z, \xi) + \lambda^T g(z, \xi) + v^T c(z), \tag{16}$$

where the tuple $\xi = (\hat{x}(t), r(t))$ collects the time varying parameters of the OCP and λ and v are Lagrange multipliers. The following quadratic programming problem (QPP) is then solved at the kth time-step

$$\begin{aligned} \min_{\Delta z} \frac{1}{2} \Delta z^T H\, \Delta z + q^T \Delta z, \\ s.t. \quad G\, z = h, \\ A\, z \leq b, \end{aligned} \tag{17}$$

where $H \approx \nabla_z^2 L(z_{k-1}, \lambda_{k-1}, v_{k-1}),\ q = \nabla_z L(z_{k-1}, \lambda_{k-1}, v_{k-1}),\ G = \nabla_z g(z_{k-1}),\ h = g(z_{k-1}),$ $A = \nabla_z c(z_{k-1}),$ and $b = -c(z_{k-1})$. The solution estimate is then updated as

$$z_k = \Delta z^* + z_{k-1}, \tag{18}$$

and the multipliers are updated as

$$v_k = v^*, \lambda_k = \lambda^*, \tag{19}$$

where $(\Delta z^*, \lambda^*, v^*)$ is the solution of the QP. Under certain assumptions, this strategy generates a stabilizing feedback law and will converge to the optimum solution of the original nonlinear program [27].

Written out explicitly, the feedback control law is computed by repeatedly solving QPs of the form:

$$\begin{aligned} \min_{x,u,s} \quad & \begin{bmatrix} \Delta u \\ \Delta x \end{bmatrix}^T \begin{bmatrix} H_u & 0 \\ 0 & H_x \end{bmatrix} \begin{bmatrix} \Delta u \\ \Delta x \end{bmatrix} + \begin{bmatrix} d_u \\ d_x \end{bmatrix}^T \begin{bmatrix} \Delta u \\ \Delta x \end{bmatrix} + \gamma_1 1^T s \\ s.t. \quad & A\Delta x + B\Delta u + g(\bar{x},\bar{u}) = 0 \\ & C\Delta x + c(\bar{x}) \leq \Gamma s \\ & P\Delta u + p(\bar{u}) \leq 0 \\ & s \geq 0 \end{aligned} \tag{20}$$

where $\Gamma = I_N \otimes 1_N$, $C = \nabla_x c(\bar{x})$, $P = \nabla_u p(\bar{u})$, $A = \nabla_x g(\bar{x},\bar{u})$, $B = \nabla_u g(\bar{x},\bar{u})$, $H_x = diag(I_{N-1} \otimes Q \ , Q_f)$, $H_u = I_N \otimes R$.

To speed up computations we can condense the problem. Since for any sequence u the state sequence x is uniquely determined A must be invertible, allowing us to write

$$\Delta x = -A^{-1}B\Delta u - A^{-1}g(\bar{x},\bar{u}) = G\Delta u + w \tag{21}$$

We can then write the condensed problem as

$$\begin{aligned} \min_{\Delta u,s} \quad & \begin{bmatrix} \Delta u \\ s \end{bmatrix}^T \begin{bmatrix} H & 0 \\ 0 & 0 \end{bmatrix} \begin{bmatrix} \Delta u \\ s \end{bmatrix} + \begin{bmatrix} d \\ \gamma 1 \end{bmatrix}^T \begin{bmatrix} \Delta u \\ s \end{bmatrix} \\ s.t. \quad & \begin{bmatrix} P & 0 \\ CG & -\Gamma \\ 0 & -I \end{bmatrix} \begin{bmatrix} \Delta u \\ s \end{bmatrix} + \begin{bmatrix} \bar{p} \\ \bar{c} + Cw \\ 0 \end{bmatrix} \leq 0, \end{aligned} \tag{22}$$

where $H = H_u + G^T H_x G$, and $d = d_u + G^T(H_x w + d_x)$. The iterates can then be updated as

$$x \leftarrow \bar{x} + G\Delta u + w, \qquad u \leftarrow \bar{u} + \Delta u. \tag{23}$$

Preliminary computational results indicate an estimated execution time of 35 ms for four QP solves. This is well within the 2 second sampling period indicating the controller is real-time feasible.

3.3 Parameter Governor Control of Multi-Vehicle Formations

Parameter governors represent a class of predictive control schemes that adjust parameters, such as gains or offsets, in nominal closed-loop control schemes in order to enforce pointwise-in-time state and control constraints and improve performance [10]. Unlike more general nonlinear MPC schemes, parameter governors are low computational complexity approaches based on a solution of a low-dimensional optimization problem. In some cases, the values of adjustable variables (parameters) can be confined to a finite set of small cardinality so that the solution can be determined by direct search. Our initial work, reported in our interim report[1], mostly focused on developing parameter governors to form and maintain a formation of n-spacecraft. The objective was to place all spacecraft onto desired closed, unforced NMTs in a relative motion frame with the correct phasing. The parameter governors adjust the target trajectory provided to each

[1]Kolmanovsky, I.V. and Girard, A.R., "Advanced predictive control for applications to autonomous vehicles and vehicle formations," Annual Performance Report for Grant FA9453-16-1-0069, 2017.

spacecraft by modifying a parameter corresponding to either a time shift or a scale shift applied to the nominal target trajectory. Hence, the two parameter governors are referred to as the Time Shift Governor (TSG) [12] and the Scale Shift Governor (SSG) [13]. Both the TSG and SSG assume linear dynamics models and are restricted to using a single parameter for each spacecraft in formation.

More recently, we have focused on generalizing the previous results to larger classes of governing algorithms and advancing theoretical results which establish performance guarantees for them. Specifically, our most recent results apply to systems with non-linear dynamics and can be used to generate formations of vehicles traveling along either forced or unforced trajectories. Additionally, the number of parameters available for each vehicle is not restricted, and a turn-based parameter update strategy is used to ensure parameter updates can be obtained quickly even for formations with a large number of vehicles and/or if non-convex constraints are present.

3.3.1 Assumptions.

The relative motion dynamics for each vehicle, $i \in \mathbb{S} = \{1,2,\cdots,q\}$, are modeled in discrete-time as

$$X_i(k+1) = f\big(k, X_i(k), u_i(k)\big) \tag{24}$$

where the function f is globally Lipschitz in its arguments, $k \in \mathbb{Z}_{>0}$ designates the discrete time instants, $X_i(k)$ is the state vector, and $u_i(k)$ are control inputs. The control inputs are given by

$$u_i(k) = u_{di}\big(k, p_i(k)\big) + u_{fi}\left(p_i(k), X_i(k), X_{di}\big(k, p_i(k)\big)\right), \tag{25}$$

where $p_i(k)$ is a vector of parameters that are adjusted by the parameter governor, u_{di} is a feed-forward term based on a nominal reference trajectory defined by nominal control input $\bar{u}_{di}(k)$ and a specified initial condition $\bar{X}_{di}^0$, and u_{fi} is a feedback term designed to track this same trajectory. Specifically,

$$\begin{aligned} u_{di}\big(k, p_i(k)\big) &= \bar{u}_{di}\big(k+\theta_i, p_i(k)\big), \\ X_{di}\big(k, p_i(k)\big) &= \bar{X}_{di}\big(k+\theta_i, p_i(k)\big), \\ \bar{X}_{di}(k+1) = f\big(k, \bar{X}_{di}(k), \bar{u}_{di}(k)\big), &\qquad \bar{X}_{di}(0) = \bar{X}_{di}^0 \end{aligned} \tag{26}$$

where θ_i is an integer specifying the desired phasing of each vehicle along its reference trajectory. The feedback law u_{fi} is continuous in its arguments and is equal to zero if the current vehicle state is equal to the current controller reference point, i.e., if $X_i(k) = X_{di}\big(k, p_i(k)\big)$. Note that the additional argument $p_i(k)$ in u_{fi}, $\bar{u}_{di}$, and $\bar{X}_{di}$ implies that the parameter governor may either modify the nominal target provided to each vehicle controller, or modify the action of the feedback portion of the control law. It is assumed that the control law $u_i(k)$ is stabilizing to the reference trajectory when any adjustments made to the parameter do not change the reference trajectory.

The overall inner-loop system is composed from   subsystems and has state, control, parameter and controller reference point vectors given by

$$X(k) = \left[X_1(k)^T, X_2(k)^T, \cdots, X_q(k)^T\right]^T,$$
$$u(k) = \left[u_1(k)^T, u_2(k)^T, \cdots, u_q(k)^T\right]^T, \tag{27}$$
$$p(k) = \left[p_1(k)^T, p_2(k)^T, \cdots, p_q(k)^T\right]^T,$$

$$X_d\big(k, p(k)\big) = \left[X_{d1}\big(k, p_1(k)\big)^T, X_{d2}\big(k, p_2(k)\big)^T, \cdots, X_{dq}\left(k, p_q(k)\right)^T\right]^T, \tag{28}$$

respectively. Pointwise-in-time constraints are imposed on the state, control and parameter of the overall system as

$$X(k) \in \mathbb{X}, \;\; u(k) \in \mathbb{U}, \;\; p(k) \in \mathbb{P}^q, \tag{29}$$

$$X(k) \in \mathbb{X}, \;\; u(k) \in \mathbb{U}, \;\; p(k) \in \mathbb{P}^q,$$

where $\mathbb{X}$, $\mathbb{U}$, and $\mathbb{P}$ are compact sets. Furthermore, the parameter set $\mathbb{P}$ is a discrete set with a finite number of elements.

3.3.2 Methods.

The parameter vector is selected by the parameter governor at each discrete-time instant to minimize, or possibly simply to decrease (when feasible) the following cost function over a horizon of T steps:

$$J(k, p(k), X(k)) = W\big(p(k)\big) + \Omega\big(k, p(k), X(k)\big), \tag{30}$$

subject to the condition that constraints are satisfied with the parameter held constant over the prediction horizon. In the cost function, the term W is the parameter cost that depends only on the parameter value for the combined system, and Ω is the incremental cost that penalizes deviation from the reference trajectory, and may depend on the parameter, control and state of the combined system. The functions W and Ω can be flexibly defined based on the desired formation, the types of parameters considered, and desired system performance. Details of the properties that W and Ω must satisfy to ensure good performance are included in Section 5.2.3 of [28] These properties are defined such that the desired formation is achieved if and only if $J = 0$.

At the initial time instant $k = 0$, an initial parameter vector is selected as any feasible solution to the following global optimization problem:

$$\min_{p(k)} J(k, p(k), X(k)) \tag{31}$$

subject to

$$X(k + \sigma | k) \in \mathbb{X}, \sigma = 0,1, \dots, T,$$

$$p(k) \in \mathbb{P}^q,$$
$$X(k|k) = X(k).$$

Note that because the parameter vector is limited to a discrete set with a finite number of elements, a feasible solution can be obtained by running a finite number of simulations and selecting the first value for $p(k)$ that satisfies constraints.

At all subsequent time-instants $k > 0$, parameters are updated using a “turn-based” strategy based on a similar strategy developed for distributed command governors [29, 30]. In the turn-based strategy, at each time instant, only vehicles in a specified “turn” (subset of vehicles) update their parameters, while all other vehicles hold their parameters fixed. The turns are defined using tools from graph color ability theory, and are determined such that all vehicles in a turn can make updates to their parameters concurrently and independently while still guaranteeing that all constraints will remain satisfied and the overall cost will not increase.

Each vehicle in the current turn updates its parameter value based on the solution to the following local optimization problem:

$$\min_{p_i(k)} J(k, p(k), X(k)) \tag{32}$$

subject to

$$X(k+\sigma|k) \in \mathbb{X}, \sigma = 0,1,\dots,T,$$
$$u(k+\sigma|k) \in \mathbb{U}, \sigma = 0,1,\dots,T-1$$
$$p(k+\sigma) = p(k), \sigma = 0,1,\dots,T,$$
$$p_i(k) \in \Gamma\big(p_i(k-1)\big),$$
$$X(k|k) = X(k),$$

where the only adjustable variables are the parameter values for the current vehicle, $p_i(k)$. Furthermore, the possible values for $p_i(k)$ are restricted to a set $\Gamma\big(p_i(k-1)\big) \subset \mathbb{P}$, which contains only the previous parameter value $p_i(k-1)$ and nearby parameter values. In this manner, updated parameter values can be obtained by running a maximum of 3^n simulations, where n is the number of elements in the vector p_i, and choosing the value that minimizes the cost. This approach is valid even if constraints are non-linear or non-convex.

Using the turn-based strategy, parameter updates are distributed over time and between spacecraft, keeping the computations required to make these updates fast. Furthermore, the computation time required to update the parameter values for any $k > 0$ is independent of the number of vehicles in formation. Complete details of the turn-based parameter update strategy are available in Section 5.2.4.2 of [28].

3.4 Safe Trajectory Generation for Satellite Inspection

In satellite inspection missions, an inspector spacecraft executes maneuvers in order to collect information about a target spacecraft. This information could be used to characterize an unknown object in space, or to diagnose the cause of a malfunction onboard the target spacecraft. Maneuvers for satellite inspection applications must be planned such that the desired information is obtained, while at the same time constraints such as thruster saturation limits and avoidance of exclusion zones are enforced to ensure feasibility and to ensure no collisions with the target spacecraft. In our previous work, reported in our recent annual report [28], an information model was developed which specifies the rate at which information about a nominal point on the target spacecraft is obtained, and three methods were formulated to generate safe (constraint satisfying) maneuvers (see [31] for additional details). In our more recent work, we have continued development of one of these techniques, the so-called “local gradient” technique, in order to better characterize the method’s ability to enforce constraints and handle disturbances, and to develop alternative rules for control switching to obtain desired performance.

3.4.1 Assumptions.

Consider two spacecraft; a non-maneuvering target spacecraft operating on a known nominal orbit, and an inspection spacecraft maneuvering near the target spacecraft. Since the majority of operational spacecraft are in low-eccentricity orbits [32], it is assumed that the target spacecraft is in a circular orbit. Hence, the motion of the inspection spacecraft relative to the target spacecraft is described by the linear time-invariant Clohessy-Wiltshire (CW) equations [23], which in discrete-time are

$$X(k+1) = AX(k) + Bu(k), \tag{33}$$

where k designates the discrete-time instants, $X(k)$ is the state vector with components corresponding to relative position and velocity, and $u(k)$ is the control vector corresponding to instantaneous velocity change, ΔV.

The goal of the inspection spacecraft is to obtain information about point $r_T \in \mathbb{R}^3$, located on the surface of the target spacecraft. Associated with this point is the unit vector $\hat{n} \in \mathbb{R}^3$, which is normal to the surface at point r_T. Both r_T and $\hat{n}$ are assumed to be static (in the relative motion frame) and known.

The rate at which information is collected is assumed to be constant over the discrete-time update period and is determined by the inspection spacecraft position at the beginning of the update period, ΔT. Hence, the information dynamics are modeled in discrete-time as

$$I(k+1) = I(k) + \dot{I}\big(X(k)\big)\Delta T. \tag{34}$$

The information rate, $\dot{I}\big(X(k)\big)$, is dependent on both distance-to-target and angle-to-target, i.e.,

$$\dot{I}\big(X(k)\big) = \dot{I}_d\big(X(k)\big)\dot{I}_\phi\big(X(k)\big). \tag{35}$$

Similar to previous work by the co-PI and her collaborators related to UAV path planning [27, 33, 34], the dependence on distance-to-target is modeled based on the Shannon channel capacity equation [35]. The angle-to-target dependence is modeled such that information is obtained only when the inspection spacecraft is within a cone defined by half-angle ϕ_{max}, central axis $\hat{n}$ and vertex r_T. The information rate is given by

$$\dot{I}(X(k)) = \dot{I}_d(X(k))\dot{I}_\phi(X(k)) = \alpha\log\left(1 + \frac{\beta}{\|d(X(k))\|_2}\right)\exp\left[\frac{-\phi(X(k))^2}{\frac{2}{9}\phi_{max}{}^2}\right] \tag{36}$$

where α and β are constants representing channel bandwidth and target visibility, respectively, $d(X(k))$ is vector from r_T to the spacecraft and $\phi(X(k))$ is the angle from $d(X(k))$ to $\hat{n}$.

Two constraints on state and control variables are considered. Firstly, the control vector magnitude is upper-bound by a parameter u_{max}, i.e.,

$$u(k) \in \mathbb{U} = \{u \mid \|u\|_\infty - u_{max} \leq 0\}. \tag{37}$$

Secondly, the distance from the inspector spacecraft to the target spacecraft is lower-bound by a parameter r_{min}, i.e.,

$$X(k) \in \mathbb{X} = \{X \mid r_{min} - \|\Phi X\|_2 \leq 0\}, \tag{38}$$

where the matrix $\Phi = [I_{3\times3}\ 0_{3\times3}]$ isolates the position components from the state vector. This constraint ensures the inspector spacecraft stays out of a spherical "keep-out zone" around the target spacecraft.

3.4.2 Methods.

A two-phase control law is developed to drive the inspector spacecraft on a path along which information about the target point can be obtained, while all constraints remain satisfied. Firstly, an analytical control law is developed based on the Local Gradient (LG) of the information collection rate, where the LG is given by

$$\frac{\partial\dot{I}}{\partial X} = \left[\frac{\partial\dot{I}}{\partial x}, \frac{\partial\dot{I}}{\partial y}, \frac{\partial\dot{I}}{\partial z}, \frac{\partial\dot{I}}{\partial\dot{x}}, \frac{\partial\dot{I}}{\partial\dot{y}}, \frac{\partial\dot{I}}{\partial\dot{z}}\right] \tag{39}$$

This LG control law is used to drive the inspection satellite on a path along which the rate of information collection is strictly increasing. Secondly, a state-feedback controller is developed to guide the inspector spacecraft to a static reference point selected by a simple Reference-governor like controller. This state-feedback controller is switched on as the inspector spacecraft approaches the target point and ensures that constraints remain satisfied.

The local gradient control law is given by

$$u(k) = u_{mag} \frac{\bar{u}}{\|\bar{u}\|_2} - B^{+}(A - I_{6\times 6})X(k) \tag{40}$$

where $\bar{u} = \left[\frac{\partial \dot{r}}{\partial X} B\right]^T$ and $B^{+} = (B^T B)^{-1} B^T$. With appropriate choice of the parameter u_{mag}, the constraint on control vector magnitude is satisfied. However, use of the local gradient control law exclusively will eventually lead to violation of the keep-out zone constraint. Consequently, the LG control law is only used until the inspection spacecraft is "sufficiently close" to the target point, where "sufficiently close" is defined in terms of control switching rules described in Section 4.4. At this point, the control law is switched to a state-feedback control law given by

$$u(k) = KX(k) + \Gamma X_d(k), \tag{41}$$

where $X_d(k)$ is the controller reference point given by $X_d(k) = \Phi^T[r_T + \delta(k)\,\hat{n}]$, $\delta(k) \in \mathbb{R}_{\geq 0}$, and $\Gamma = [\Phi(I_{6\times 6} - [A + BK])^{-1} B]^{-1}\Phi$. Under the action of this state-feedback control law, the inspector spacecraft will asymptotically approach $X_d(k)$ if $X_d(k)$ is held fixed.

The parameter $\delta(k) \in \mathbb{R}_{\geq 0}$, is determined by considering the following optimization problem at each time instant k, over a prediction horizon of T discrete-time steps:

$$\min_{\delta(k)} \delta(k) \tag{42}$$

subject to

$$\begin{gathered} X(k+\sigma|k) \in \mathbb{X}, \sigma = 0,1,\dots,T, \\ u(k+\sigma|k) \in \mathbb{U}, \sigma = 0,1,\dots,T-1 \\ \delta(k+\sigma|k) = \delta(k), \sigma = 0,1,\dots,T-1, \\ \delta(k) \geq 0, \\ X(k|k) = X(k). \end{gathered}$$

To quickly obtain a reasonable approximation to the exact solution to this non-convex optimization problem, a direct search is carried out over $\delta(k) \in \{0, \nu, 2\nu, \cdots\}$ for some small step size $\nu > 0$, and selecting $\delta(k)$ to be the smallest feasible value.

3.5 Waypoint following MPC

Motivated by applications to agile imaging satellites that must capture as many imaging sites as possible in minimum time [36], we consider a problem in which a spacecraft's attitude must follow a series of prescribed waypoints and reach each waypoint in minimum time. In addition, the spacecraft attitude trajectory must avoid entering the specified exclusion zones in order to protect sensitive measurement equipment onboard the spacecraft.

To improve robustness to unmodeled dynamics and disturbances, rather than pursuing an open-loop solution, we implement a Model Predictive Control (MPC) strategy in which the first element of the solution sequence is applied to the spacecraft and the solution is then recomputed, with the state resulting after one step used as the initial condition [37, 38]. Our MPC design is based on linearizing and converting to discrete-time the continuous-time nonlinear attitude dynamics model of the spacecraft, and then formulating a Mixed-Integer Linear Program (MILP) [39]. In this MILP, binary integer variables are used to indicate whether the trajectory has reached the target set around the destination waypoint at a given time instant, and these binary integer variables are optimized along with the control inputs over the prediction horizon. Such an approach can be extended to accommodate exclusion zone avoidance requirements that can be encoded with the help of additional binary integer variables and constraints in the Mixed-Integer Linear Program MILP.

In scenarios where a prescribed waypoint sequence is given, the minimum-time MPC solution is applied to reach the target sets corresponding to each waypoint in turn until the target set for the final waypoint is reached. The switching from the previous waypoint to the next waypoint in the sequence is effected upon reaching the target set of the previous waypoint, and a prediction horizon sufficient to reach the next waypoint is estimated. Our simulations, based on the nonlinear spacecraft attitude dynamics model with disturbances, demonstrate that the controller is able to successfully track the sequence of waypoints without violating the exclusion zone constraints.

3.5.1 Assumptions

Consider a discrete-time nonlinear system with the model given by

$$\boldsymbol{x}_{k+1} = f(\boldsymbol{x}_k, \boldsymbol{u}_k), \tag{43}$$

where $k \in \mathbb{Z}_{\geq 0}$ denotes the discrete-time instant, $\boldsymbol{x}_k \in \mathbb{R}^{n_x}$ denotes the state and $\boldsymbol{u}_k \in \mathbb{R}^{n_u}$ denotes the control input. Suppose the control constraints are given by $\boldsymbol{u}_k \in U$, where U is a compact set. We let $\{\boldsymbol{u}_k\} \in U_{seq}$ denote control sequences with elements $\boldsymbol{u}_k \in U$. We also consider control policies which are mappings of the form $\pi: \mathbb{R}^{n_x} \rightarrow \mathbb{R}^{n_u}$. A control policy is admissible if the range of this mapping is the subset of U. The set of admissible control policies is denoted by U_{pol}.

Let $C \subset \mathbb{R}^{n_x}$ be a specified target set and let τ be the first time instant at which the trajectory enters C,

$$\tau(\boldsymbol{x}_0, \{\boldsymbol{u}_k\}) = \inf\{k\colon \phi_{\{\boldsymbol{u}_k\}}(k, \boldsymbol{x}_0) \in C, k \in \mathbb{Z}_{\geq 0}\}, \tag{44}$$

where $\phi_{\{\boldsymbol{u}_k\}}(k, \boldsymbol{x}_0)$ denotes the solution of the system model with the initial condition $\boldsymbol{x}_0$ at the time instance $k \in \mathbb{Z}_{\geq 0}$ and under an admissible sequence $\{\boldsymbol{u}_k\}$. When $\boldsymbol{x}_0$ and $\{\boldsymbol{u}_k\}$ are clear from the context, we will use $\boldsymbol{x}_k$ to denote $\phi_{\{\boldsymbol{u}_k\}}(k, \boldsymbol{x}_0)$. Note that for a given $\{\boldsymbol{u}_k\}$, $\tau(\boldsymbol{x}_0, \{\boldsymbol{u}_k\})$ may not exist; in such a case, we set $\tau(\boldsymbol{x}_0, \{\boldsymbol{u}_k\}) = +\infty$.

The minimum-time problem to reach the target C is now formulated as

$$\tau(\boldsymbol{x}_0, \{\boldsymbol{u}_k\}) \rightarrow \min_{\{\mathbf{u}_k\} \in U_{seq}} (\boldsymbol{x}_0, \{\boldsymbol{u}_k\}). \tag{45}$$

The value function of this problem is denoted by $\tau_{min}(\boldsymbol{x}_0)$.

3.5.2 Methods.

Let the control constraint set U and the target set C be polyhedral, and suppose the model is linear, i.e.,

$$\begin{gathered} U = \{\boldsymbol{u} \in \mathbb{R}^{n_u} : \boldsymbol{\Gamma u} \le \gamma, \gamma \in \mathbb{R}^{n_\gamma}\}, \\ C = \{\boldsymbol{x} \in \mathbb{R}^{n_u} : \ \boldsymbol{Hx} \le \boldsymbol{h}, \boldsymbol{h} \in \mathbb{R}^{n_x}\}, \\ f(\boldsymbol{x}_k, \boldsymbol{u}_k) = \boldsymbol{Ax}_k + \boldsymbol{Bu}_k + \boldsymbol{d}. \end{gathered} \tag{46}$$

Consider the following optimization problem,

$$\sum_{k=\tau_{lb}(\boldsymbol{x}_0)}^{N} \delta_k \to \min_{\{\delta_k\},\{\boldsymbol{u}_k\}} \ , \tag{47}$$

subject to

$$\begin{gathered} \boldsymbol{x}_{k+1} = \boldsymbol{Ax}_k + \boldsymbol{Bu}_k + \boldsymbol{d}, \\ \boldsymbol{Hx}_k \le \boldsymbol{h} + M\mathbf{1}_{n_h}\delta_k, \\ \delta_k \in \{0, 1\}, \\ \Gamma\boldsymbol{u}_k \le \gamma, k = 0, 1, \dots, N-1, \\ \delta_{k+1} \le \delta_k, \end{gathered}$$

where $\boldsymbol{Hx}_k$ and $\boldsymbol{h}$ define the polyhedral target set C, $\mathbf{1}_{n_h}$ is a $n_h \times 1$ vector of ones, δ_k is a binary decision variable used to relax the inequality constraint, and $\tau_{lb}(\boldsymbol{x}_0) \in \mathbb{Z}_{\ge 0}$ denotes a known lower bound on minimum time; this can be estimated by a method such as solving the completely relaxed conventional linear program. For $\boldsymbol{x} \in C$, $\boldsymbol{Hx}_k \le \boldsymbol{h}$ is satisfied and $\delta_k = 0$; otherwise, $\delta_k = 1$. The additional constraint $\delta_{k+1} \le \delta_k$ ensures that once the target set is reached, then the state remains inside the target set for all future time steps. This problem is a MILP that can be solved using standard numerical algorithms.

Suppose the solution to the proposed minimum time optimal control problem exists for a given $\boldsymbol{x}_0$. Then for all sufficiently large M and N, for the solution sequence $\{\boldsymbol{u}_k^*\}$, it holds that $\tau(\boldsymbol{x}_0, \{\boldsymbol{u}_k^*\}) = \tau_{\{min\}}(\boldsymbol{x}_0)$. The open loop solution sequence $\{\boldsymbol{u}_k^*\}$, determined for the given $\boldsymbol{x}_0$ on the basis of the linearized model, if applied to a nonlinear model, may not lead to a trajectory that reaches the target set due to the model mismatch. To improve the robustness of the solution, the receding horizon control principle is used as in model predictive control. Hence, we define a feedback law based on the first move of the solution sequence $\{\boldsymbol{u}_k^*\}$, as

$$\boldsymbol{u}_{MPC}(\boldsymbol{x}_0) = \boldsymbol{u}_0^*, \qquad \big(\boldsymbol{u}_0^* = \boldsymbol{u}_0^*(\boldsymbol{x}_0)\big). \tag{48}$$

Such a solution is referred to as the minimum-time MPC feedback law.

The minimum-time MPC can be applied to waypoint following problems in a straightforward manner: Given a sequence of waypoints and associated target sets, one commands each target set sequentially to the minimum time MPC controller until it is reached and then a switch to the next waypoint in the prescribed waypoint sequence is initiated.

4. RESULTS AND DISCUSSION

4.1 Invariance-based constrained spacecraft relative motion planning

A virtual net is formed from 68 NMTs, including 50 closed NMTs (36 elliptical, 7 line-segment and 7 stationary point), and 18 open NMTs (12 helical and 6 line-segment). These NMTs are selected such that they are contained in, and evenly spaced throughout, a box of $2 \times 3 \times 4$ km in the $x, y,$ and z directions, respectively, in Hill's frame, centered at the origin. The portion of the virtual net corresponding only to closed NMTs has 50 nodes, while the entire virtual net (including both open and closed NMTs) has 2686 nodes. Parameters used in simulations are shown in Table 1.

Figure 1 shows an example trajectory connecting a stationary-point NMT to an elliptical NMT, planned only using the portion of the virtual net corresponding to closed NMTs. The spacecraft travels to two intermediate elliptical NMTs before reaching the final NMT. The total control cost, calculated as $J = \Delta T \sum_0^{k_{final}} \|u(k)\|_1$, of this trajectory is 453 N·s. Figure 2 shows an example trajectory connecting the same two NMTs planned using the entire virtual net, including both open and closed NMTs. The spacecraft travels to two intermediate NMTs, including one elliptical NMT, and an open before reaching the final NMT. The total cost of this trajectory is 316 N·s. These simulations illustrate that including closed NMTs in the virtual net allows for a more diverse range of trajectories, and also may result in improved fuel efficiency. These benefits come at the expense of additional computations required to form the virtual net, resulting from the large increase in the number of nodes when closed NMTs are included.

Table 1. Parameters used for Invariance-based Constrained Spacecraft Relative Motion Planning Simulations

Parameter	Units	Value
Spacecraft mass	kg	140
Nominal orbital radius	km	7728.137
Discrete-time update period	sec	$\Delta T = 61.16$
Maximum admissible control	N	$u_{max} = 2$
Center of exclusion zone	km	$s = [0\ 0\ 0]^T$
Center of exclusion zone	-	$S = \text{diag}(400, 40, 400)$
LQR State weighting matrix	-	$Q = 100\text{diag}(1,1,1,1 \times 10^5, 1 \times 10^5, 1 \times 10^5)$
LQR Control weighting matrix	-	$R = 2 \times 10^7 \text{diag}(1,1,1)$
Ellipsoidal set shape matrix	-	Solution to discrete-time Riccati eq'n in LQ problem

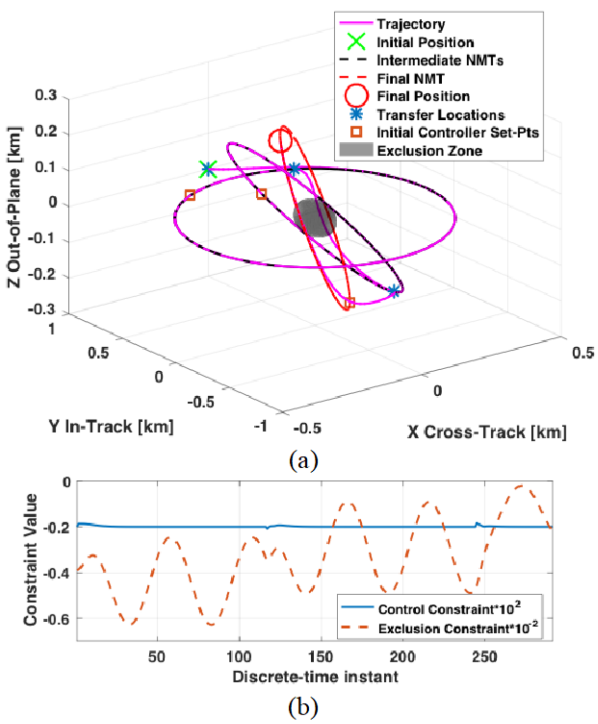

Figure 1. Example Trajectory Planned using only Closed NMTs. (a) Trajectory, (b) Constraints Calculated Along the Trajectory. Constraints are Satisfied if they are Less-than-or-equal-to zero

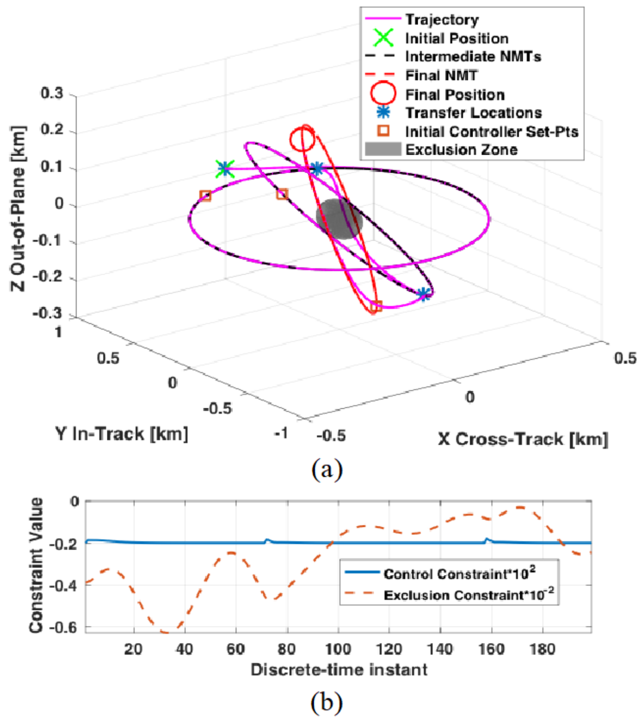

Figure 2. Example Trajectory Planned using Open and Closed NMTs. (a) Trajectory, (b) Constraints Calculated along the Trajectory. Constraints are Satisfied if they are Less-than-or-equal-to zero

4.2 NMPC for Spacecraft Control

The NMPC controller described in Section 3.2 is implemented in Simulink in preparation for hardware testing on AFRL's attitude testbed platform. The C code for suitable real-time implementation is automatically generated for rapid prototyping hardware using the Simulink real-time workshop. Five scenarios were devised and the simulation results of which are presented below. Implementation on the REBEL testbed was attempted but unforeseen difficulties during the window of available time prevented any real results from being available.

The Simulink simulations consist of five cases which represent the order in which hardware testing would be done: 1) Verify implementation without constraints, 2) Implement control constraints, 3) Impose constraints on the Euler angle rates, 4) Impose constraints on the Euler angles, and 5) Impose a non-linear inclusion cone constraint on the orientation. A constant nonzero disturbance, d, is applied to the plant model to demonstrate the effectiveness of the rate-based formulation. For the simulations presented below, the worst-case runtime for the controller algorithm is approximately 1.6 sec. The sampling time of the system is two seconds and the prediction horizon is ten steps.

Figure 3 is case one, which is mainly considered as a case that would verify that the NMPC package is properly installed and that all signals are handled properly. In this case, the controller moves the orientation of the platform a small distance away and holds the new reference. This case was the only one during the AFRL's attitude testbed implementation attempt.

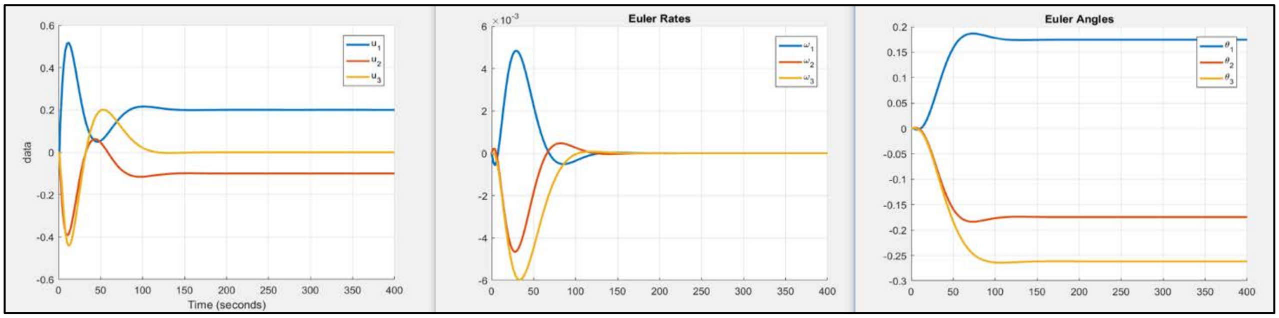

Figure 3. Simulation Results using the NMPC Algorithm with no Constraints. From left to right: Input Trajectory, Euler Rates, and Euler Angles

Figure 4 is case two, where input constraints are added to demonstrate enforcement of box constraints.

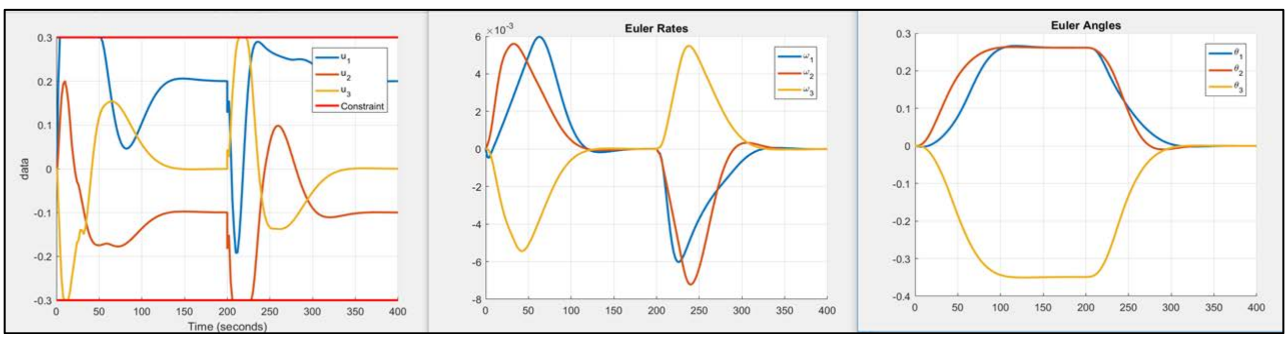

Figure 4. Simulation Results using the NMPC Algorithm with Input Constraints. From left to right: Input Trajectory, Euler Rates, and Euler Angles

Figure 5 is case three, where Euler rate constraints are implemented to demonstrate the ability to regulate the speeds.

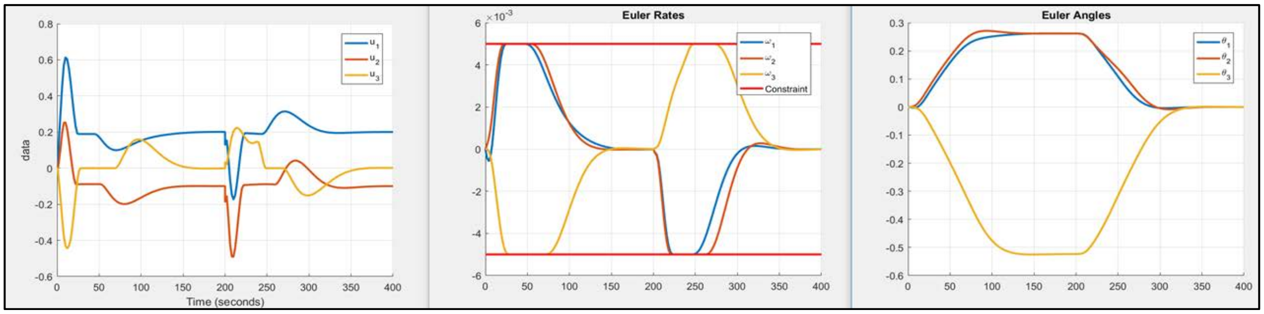

Figure 5. Simulation Results using the NMPC Algorithm with Euler Rate Constraints. From left to right: Input Trajectory, Euler Rates, and Euler Angles

Figure 6 is case four, where Euler angle constraints are implemented. The concern is that without a sufficiently long enough window, the controller may approach the state constraints with too much momentum to maintain feasibility.

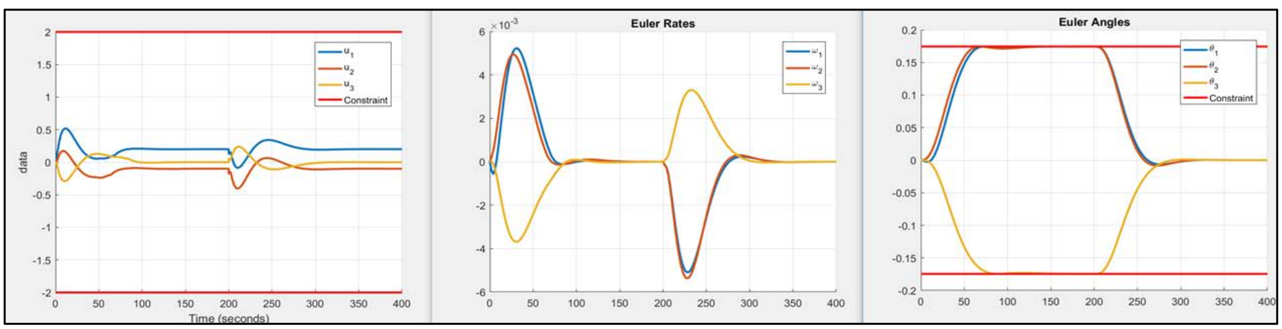

Figure 6. Simulation Results using the NMPC Algorithm with Euler Angle Constraints. From left to right: Input Trajectory, Euler Rates, and Euler Angles

Figures 7 and 8 are for case five, where an instrument inclusion cone constraint is imposed. This constraint is inherently non-linear, but convex which the NMPC implementation is able to handle.

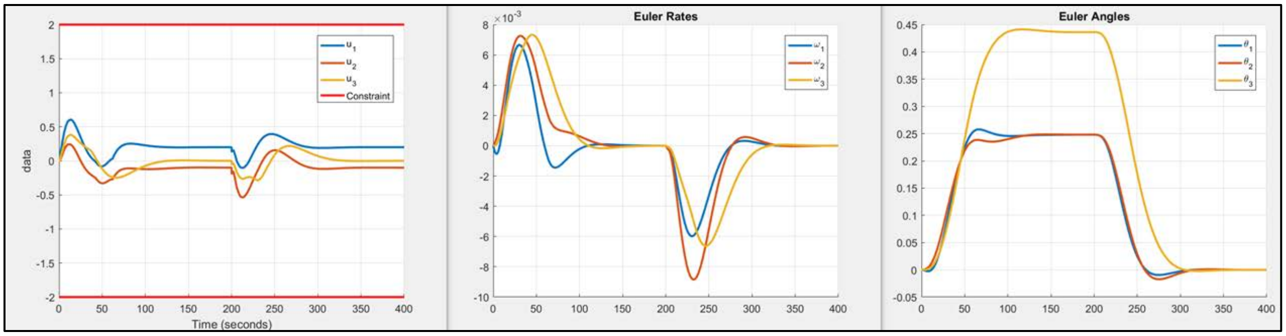

Figure 7. Simulation Results using the NMPC Algorithm with Instrument Inclusion Cone Constraint. From left to right: Input Trajectory, Euler Rates, and Euler Angles.

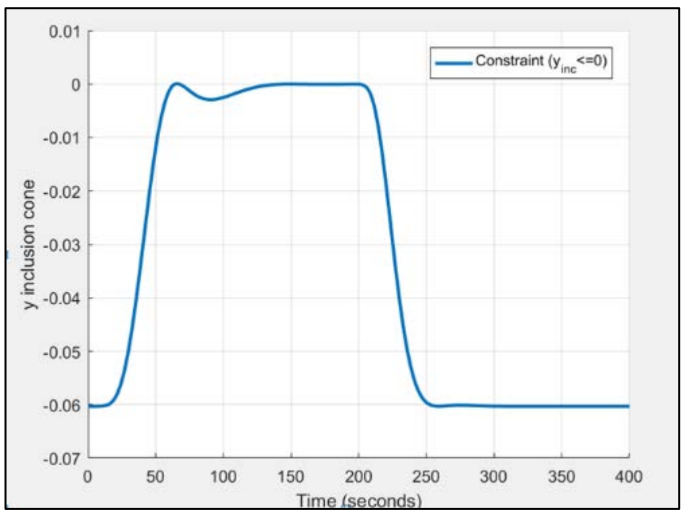

Figure 8. Inclusion Cone Constraint During Simulation of Case Five

These tests demonstrate the ability of the NMPC controller to handle the five cases suggested for testing on the AFRL's attitude testbed platform.

4.3 Parameter Governor Control of n-vehicle Formations

Both theoretical and experimental results have been obtained. The theoretical results provide guarantees that the parameter governor is able to generate and maintain desired formations consisting of n vehicles. These theoretical results are applicable to a broad class of vehicles (or systems) whose dynamics are modeled using non-linear equations, and handle the general case where a vector of parameters is calculated and applied for each vehicle in formation. Note that the previously reported theoretical results for the Time Shift Governor TSG and Scale Shift Governor SSG [28], which utilized linear dynamics and scalar parameters, are specialized cases of the more general results reported here.

Simulation results have also been obtained for a combined TSG/SSG that adjusts two parameters for each spacecraft, corresponding to both time- and scale-shifts applied to the nominal reference trajectories. These results demonstrate that utilizing this combined approach with multiple parameters may provide better performance compared to either the TSG or SSG alone.

4.3.1 Theoretical Results.

The main theoretical results for the parameter governor are summarized here. Detailed descriptions of the required assumptions, and detailed proofs for each result, are available in Section 5.2.5 of [28].

Firstly, Proposition 1 establishes the existence of a finite, sufficiently long prediction horizon $T^* \in \mathbb{Z}_{>0}$ such that constraint satisfaction need only be verified over this horizon:

Proposition 1 (Proposition 5.1 in [28]): There exists $T^* \in \mathbb{Z}_{>0}$ such that, for $(X^0, p) \in \mathbb{D}(k)$, $k \in \mathbb{Z}_{\geq 0}$, if $X(k+\sigma|k,p,X^0) \in \mathbb{X}$ and $u(k+\sigma|k,p,X^0) \in \mathbb{U}$ for $\sigma \in \mathbb{Z}_{[0,T^*]}$, then $X(k+\sigma|k,p,X^0) \in \mathbb{X}$ and $u(k+\sigma|k,p,X^0) \in \mathbb{U}$ for all $\sigma > T^*$.

Secondly, Proposition 2 establishes that utilizing the turn-based parameter update strategy, the total cost J is non-increasing:

Proposition 2 (Proposition 5.2 in [28]): Suppose the parameter $p(k)$ is updated using the turn-based parameter update strategy, and the prediction horizon satisfies $T \geq T^*$, where T^* is defined in Proposition 1. Then, the cost is non-increasing, i.e., $J\big(k+1, p(k+1), X(k+1)\big) \leq J\big(k+1, p(k), X(k+1)\big)$.

Finally, Theorem 2 establishes that the parameter governor will establish and maintain the desired formation of vehicle from any feasible initial condition.

Theorem 2 (Theorem 5.1 in [28])**:** Suppose Assumptions (A1)-(A5) hold, the prediction horizon satisfies $T \geq T^*$, where T^* is defined in Proposition 1, and the parameter $p(k)$ is determined using the turn-based parameter update. Then, the following properties hold:

a. $X(k)$ remains feasible, $X(k) \in \mathbb{X}$ and $u(k) \in \mathbb{U}$ for all $k \geq 0$.
b. $\Omega\big(k, p(k), X(k)\big) \to 0$ as $k \to \infty$.
c. $u_i(k) \to 0$ as $k \to \infty$ for $i = 1, 2, \ldots, q$.
d. $e_i(k) = X_i(k) - X_{di}(k, p_i(k)) \to 0$ as $k \to \infty$ for $i = 1, 2, \ldots, q$.
e. There exists $\tilde{k} > 0$ such that $W(g(k)) = 0$ for all $k \geq \tilde{k}$
f. $J\big(k, p(k), X(k)\big) \to 0$ as $k \to \infty$.

Additional theoretical results show that if certain other mild assumptions hold, then the parameter converges to a limit in finite time and, therefore, the parameter governor becomes inactive. See Corollaries 5.1-5.3 in [28] for details.

4.3.2 Simulation Results.

In previous work, we have developed simulations showing that both the TSG and SSG are capable of generating formations of spacecraft travelling along elliptical NMTs at a desired phasing [24, 12]. More recently, we have developed simulations demonstrating that a combined TSG/SSG which adjusts parameters corresponding to both time- and scale-shifts applied to the nominal reference trajectories may provide better performance compared to either parameter governor. This combined SSG/TSG implementation is supported by the theoretical results described above, which allow for multiple adjustable parameters per spacecraft.

In the combined SSG/TSG simulations, spacecraft dynamics are modelled using the linear time-invariant CW equations [23]. A static state-feedback LQR control law is utilized with control inputs corresponding to instantaneous velocity change, Δ . Parameters used in the simulations are shown in Table 2. The basic idea behind the combined TSG/SSG implementation is to choose an appropriate set of initial parameters, then, first engage the TSG and run until the TSG parameter cost goes to zero. Next, the SSG is engaged and run until the SSG parameter cost, and finally the total cost, reach zero.

Table 2. Parameters used for TSG and SSG Simulations

Parameter	**Units**	**Value**
Parameter set for τ_i	-	$\tau_i = \{0,1, \dots ,49\}$
Parameter set for g_i	-	$g_i = \{0.5, 0.6, \dots ,5.4\}$
Nominal circular orbit radius	km	R_0=6,728
Relative phase shift parameters	-	$\theta_1 = 16, \theta_2 = 0, \theta_3 = 33$
LQR state weighting matrix	-	$Q = diag(1, 1, 1, 0.001, 0.001,0.001)$
LQR control weighting matrix	-	$R = 1 \times 10^8 diag(1,1,1)$
Discrete-time update period	Sec	$\Delta T = 109.84$ sec
Prediction horizon	-	75 discrete-time steps

In the example simulation shown below, the spacecraft are initially located at initial conditions given by

$$, X_1(0) = [0, -12,0,0,0,0]^T,$$
$$X_2(0) = [0, -10,0,0,0,0]^T,$$
$$X_3(0) = [0, -8, 0,0,0,0]^T$$

where units for position are km. The objective is to place the spacecraft on three concentric elliptical NMTs, separated in phase by approximately 120^o. Note that from these initial conditions, it is not possible to generate the desired formation using either the TSG or SSG alone[2], however the desired formation is attained using the combined TSG/SSG approach.

Simulation results are shown in Figure 9. Figure 9a demonstrates that the combined SSG/TSG enforces all constraints. Figure 9b shows how the combined parameter governor makes adjustments first to the time-shifts, τ_i, and then to the scale shifts g_i, such that W_τ and W_g both converge to 0, and Figure 9c shows that the total cost also goes to 0 for large k, and hence the desired formation is attained. Figure 9d shows spacecraft trajectories.

[2] In the SSG case, no feasible initial parameter values exist. In the TSG case, initial parameter values exist, but the TSG is unable to converge to the desired formation.

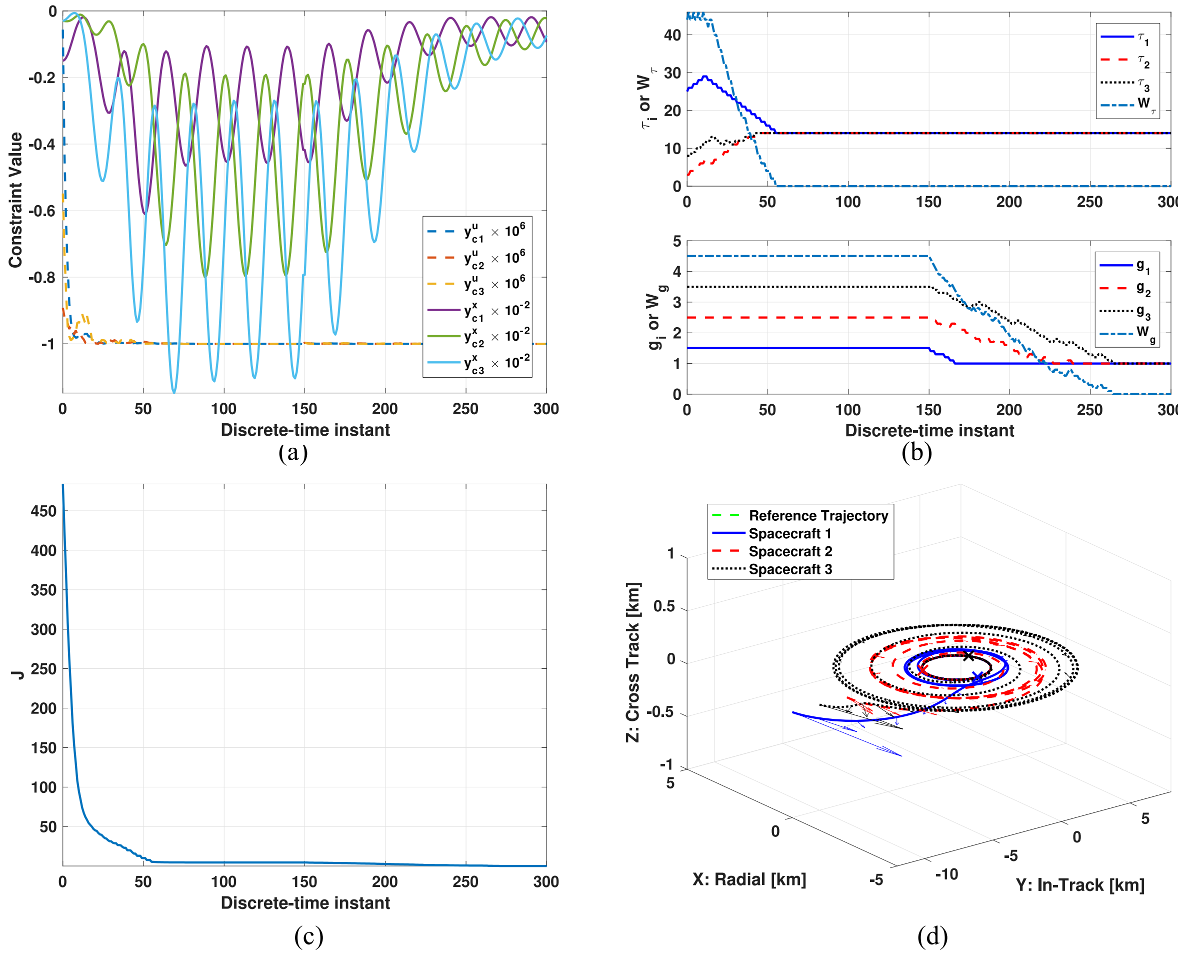

Figure 9. Demonstration of the combined SSG/TSG. (a) Constraints with Combined SSG/TSG Active, (b) Parameters, $W_\tau(\tau(k))$ and $W_g(g(k))$ vs. time, (c) Cost Parameter, (d) Spacecraft Trajectories. For Constraints, solid lines Denote Separation Distance Constraints and Dashed lines Denote Control. Constraints are Satisfied if they are Less-than-or-equal-to zero. For Trajectories, Arrows Represent ΔV Direction. X's Denote Final Spacecraft Positions

4.4 Safe Trajectory Generation for Satellite Inspection

Simulations case studies were performed to illustrate the implementation of the two-phase control law for satellite inspection described in Section 3.4.2. Table 3 shows parameters used in simulations. The control law is switched from the LG control law to the state-feedback control law at the first time-instant k when the inspector spacecraft state vector satisfies a distance criterion given by

$$\|\Phi X(k)\|_2 \leq 0.05 \text{ km}, \tag{49}$$

and an angle criterion given by

$$\phi(k) \leq 5 \text{ deg}, \tag{50}$$

where $\phi(k)$ is the angle between the vector from the target point to the inspector spacecraft and $\hat{n}$.

Table 3. Parameters used in Simulations

Parameter	**Units**	**Value**
Target spacecraft orbital radius	km	$R_0 = 6828.137$
Discrete-time update period	sec	$\Delta T = 10$
LQR state weighting matrix	-	$Q = diag(10, 10, 10, 0.01, 0.01, 0.01)$
LQR control weighting matrix	-	$R = 1 \times 10^8 diag(1,1,1)$
Maximum control limit	km/sec	$u_{max} = 0.001$
Keep-out-zone radius	km	$r_{min} = 0.02$
Target point	km	$r_T = [0.001, 0, 0.001]^T$
Target normal vector	km	$\hat{n} = \left[\frac{1}{\sqrt{2}}, 0, \frac{1}{\sqrt{2}}\right]^T$
Information collection parameters	-	$\alpha = 0.1, \beta = 0.0001$
Maximum angle for info. Collection	rad	$\phi_{max} = \frac{\pi}{6}$
Prediction horizon used to determine $\delta(k)$	Discrete-time steps	$T = 100$
Step size used to determine $\delta(k)$	km/sec	$\nu = 0.001$

Figure 10 shows three trajectories using this switched control law starting from three different initial conditions. Figure 10a shows the complete trajectories, whereas Figure 10b shows a close-up of these trajectories near the keep-out-zone. The information collection rate at each discrete-time instant along these trajectories is shown in Figure 10c. The time-instants where the control law switches from the LG law to the state-feedback law are shown as dashed black lines. The total information obtained along these trajectories is shown in Figure 10d, and constraints are plotted in Figure 10e and Figure 10f. These plots show that constraints are satisfied along the trajectories.

More extensive simulations in Section 4.4 of [28] show that the proposed LG/State-feedback control law is robust to the choice of initial condition. Furthermore, in Section 4.5 of [28], different choices for parameter values such as u_{mag} and ΔT as well as different control switching criteria are analyzed through simulation case studies to assess their effect on trajectories, control (fuel) use and information collection. The conclusion from these cases studies is that reducing the value for u_{mag} is most effective in reducing overall fuel usage while eliminating the distance criteria used to determine the time to switch to the state-feedback control law is most effective in increasing the amount of information obtained over a given time period.

Simulations also show that the proposed method is robust to sufficiently small disturbances. Figure 11 shows trajectories starting from the same initial conditions as Figure 10. For the trajectories in Figure 11, a disturbance term $Bw(k)$ is added to the dynamics at each time-step, where $w(k)$ is a disturbance vector randomly assigned from a uniform distribution over an infinity-norm ball centered at the origin with a radius of 0.025 m/sec. Comparing Figure 11a to Figure 10a it is evident that the disturbances have minimal effect on the trajectories when the LG control law is used. Furthermore, as shown in Figure 11b, when disturbances are included, closed-loop trajectories converge to a small region around the controller reference point, rather than exactly to the reference point. As long as the controller reference point is chosen to be “sufficiently far” from the keep-out-zone, the exclusion zone constraint remains satisfied. Details of the implementation with disturbances are available in Section 4.6 of [28].

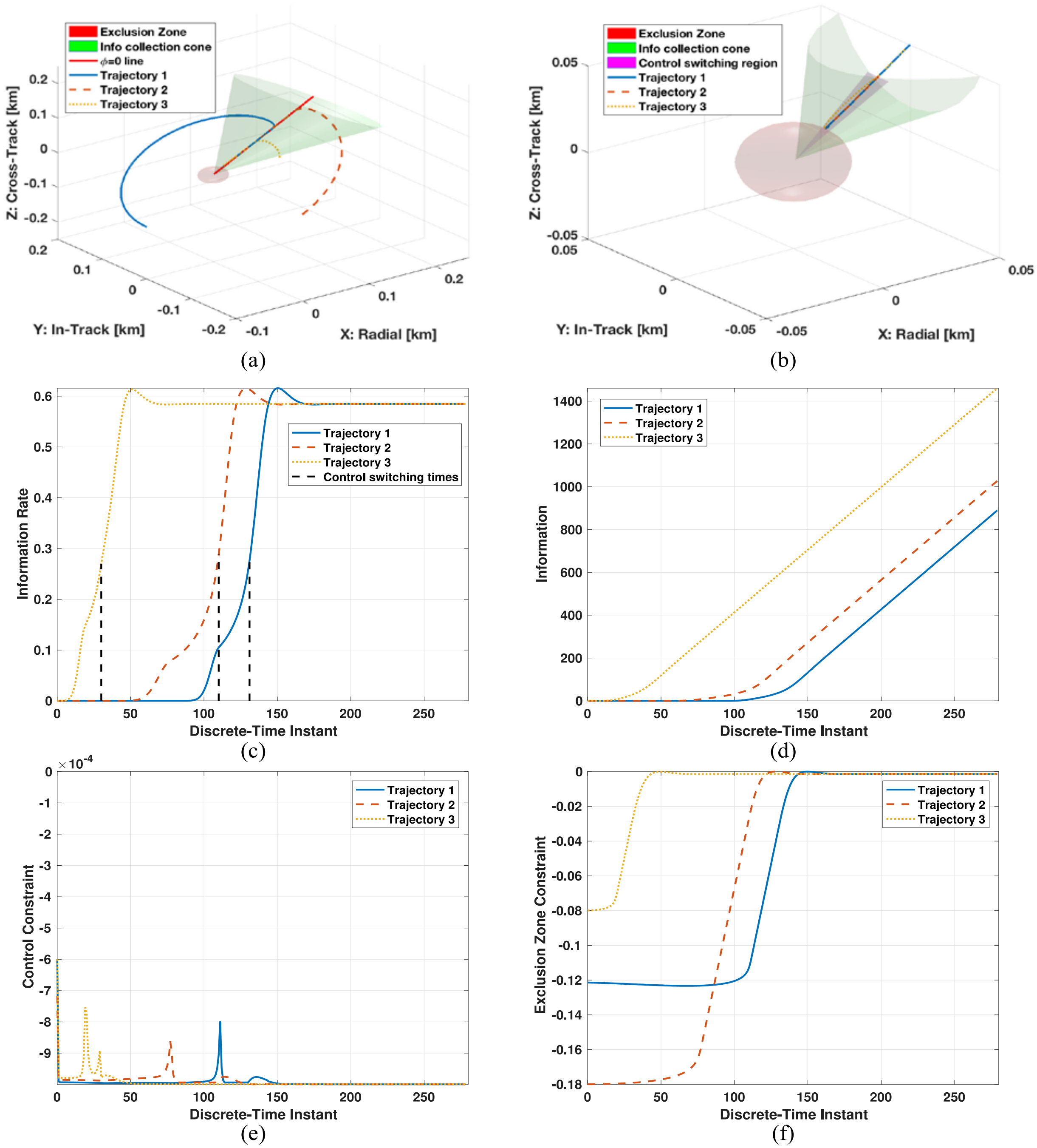

Figure 10. Example Trajectories and Associated data.
(a) Complete Trajectories, (b) Close-up of Trajectories, (c) Information rate (d) Total Information Collected, (e) Control Constraint, (f) Keep-out-zone constraint. Constraints are Satisfied if the Values are Less-than-or-equal-to zero

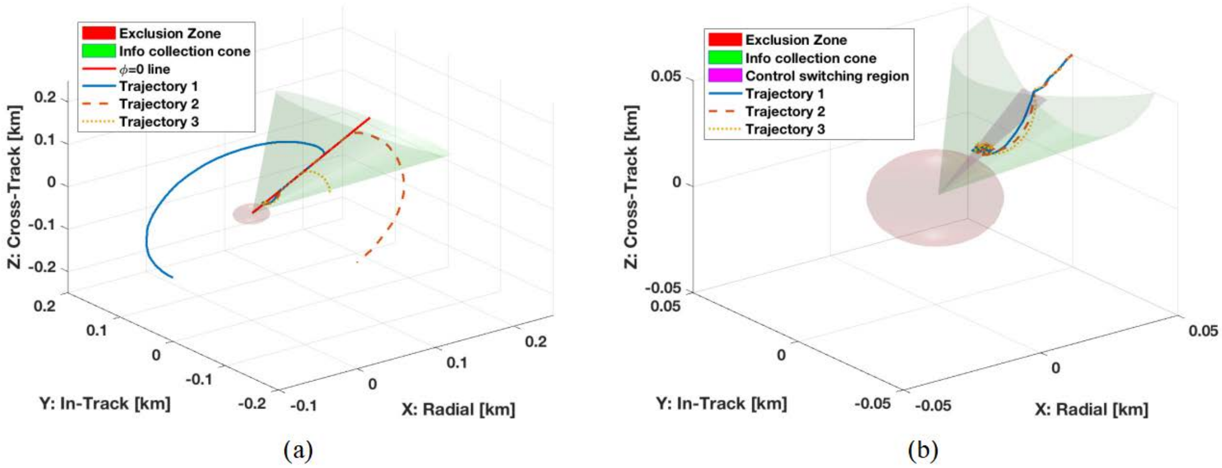

Figure 11. Example Trajectories with Disturbances. (a) Complete Trajectories, (b) Close-up of Trajectories

4.5 Minimum Time MPC Application to Spacecraft Attitude Waypoint Following

Consider a nonlinear model for the spacecraft attitude dynamics (see e.g. [40] for details) given by,

$$\begin{bmatrix} \dot{\phi} \\ \dot{\theta} \\ \dot{\psi} \end{bmatrix} = \mathbf{C}_{\phi\theta}^{-1} \left(\begin{bmatrix} \omega_1 \\ \omega_2 \\ \omega_3 \end{bmatrix} + n \begin{bmatrix} c_\theta s_\psi \\ s_\phi s_\theta s_\psi + c_\phi c_\psi \\ c_\phi s_\theta s_\psi - s_\phi c_\psi \end{bmatrix} \right), \tag{51}$$

where

$$\mathbf{C}_{\phi\theta}^{-1} = \left(\frac{1}{c_\theta} \right) \begin{bmatrix} c_\theta & s_\phi s_\theta & c_\phi s_\theta \\ 0 & c_\phi c_\theta & -s_\phi c_\theta \\ 0 & s_\phi & c_\phi \end{bmatrix},$$

and

$$\begin{aligned} \dot{\omega}_1 &= J_{23}(\omega_2\omega_3 - 3n^2 c_\phi s_\phi c_\theta^2) + \frac{u_1}{J_1}, \\ \dot{\omega}_2 &= J_{31}(\omega_3\omega_1 + 3n^2 c_\phi c_\theta s_\theta) + \frac{u_2}{J_2}, \\ \dot{\omega}_3 &= J_{12}(\omega_1\omega_2 + 3n^2 s_\phi c_\theta s_\theta) + \frac{u_3}{J_3}, \end{aligned}$$

where $J_1 = 20\ kg.\ m^2$, $J_2 = 50\ kg.\ m^2$, $J_3 = 30\ kg.\ m^2$ are principal moments of inertia, $J_{12} := (J_1 - J_2)/J_3$, $J_{31} := (J_3 - J_1)/J_2$, and $J_{23} := (J_2 - J_3)/J_1$, and n represents low-Earth orbital mean motion. The three Euler angles (roll ϕ, pitch θ, and yaw ψ) represent the orientation of the spacecraft body fixed frame with respect to the local-vertical/local-horizonal (LVLH) frame. The control inputs are moments u_1, u_2, u_3 about each body fixed axis.

The linearized model about the LVLH-frame equilibrium $\boldsymbol{x}_e = [0, 0, 0, 0, -n, 0]^T$ takes the form,

$$\mathbf{A} = \begin{bmatrix} 0 & 0 & n & 1 & 0 & 0 \\ 0 & 0 & 0 & 0 & 1 & 0 \\ -n & 0 & 0 & 0 & 0 & 1 \\ -3n^2 J_{23} & 0 & 0 & 0 & 0 & -nJ_{23} \\ 0 & 3n^2 J_{31} & 0 & 0 & 0 & 0 \\ 0 & 0 & 0 & -nJ_{12} & 0 & 0 \end{bmatrix}, \quad \mathbf{B} = \begin{bmatrix} & \mathbf{0}_{3\times 3} & \\ J_1^{-1} & 0 & 0 \\ 0 & J_2^{-1} & 0 \\ 0 & 0 & J_3^{-1} \end{bmatrix}, \quad d = 0. \tag{52}$$

We convert the linearized model to discrete-time assuming a zero-order hold with sampling period of $\Delta T = 0.5$ seconds.

The closed-loop trajectories generated by the minimum-time MPC when applied to the continuous-time nonlinear spacecraft attitude dynamics model are shown in Figures 12a and 12b. The spacecraft follows a sequence of two waypoints for which the target sets are shown in Figures 12a and 12b by the rectangular boxes and horizontal dashed lines, respectively. Note that the waypoints are only defined in the roll-pitch-yaw subspace; the angular velocity subspace is left free. The saturation constraints on the control moments are given by $|u_i| \leq 0.2$ Nm, $i = 1, 2, 3$. Random unmeasured disturbance torques sampled from the uniform distribution over the interval [-0.01, 0.01] have been added to the control moments about each axis to represent actuation errors. As observed from the simulated trajectories, the minimum-time MPC controller designed on the linearized discrete-time model is able to track the specified waypoints while respecting control constraints even when applied to the full non-linear continuous-time model and when disturbance torques are present.

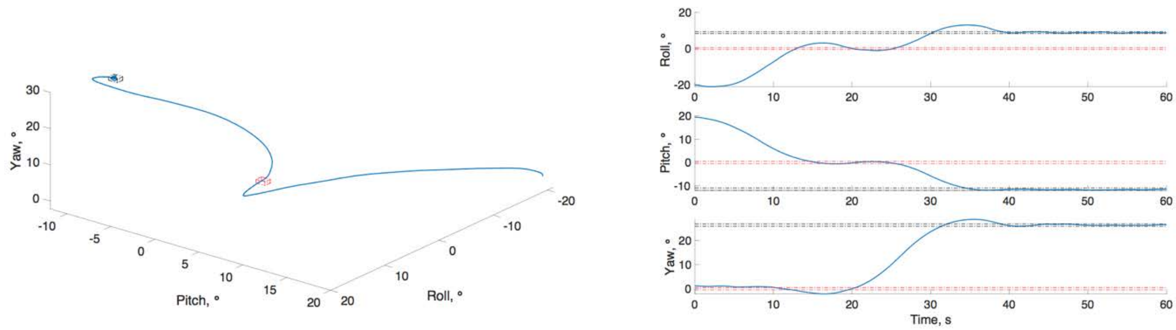

(a) (b)

Figure 12. Simulated Trajectories with Disturbances for the Minimum-time MPC Controller with 2 waypoints. (a) Roll-Pitch-Yaw Trajectory in 3D, (b) Separated Roll-Pitch-Yaw trajectories

Exclusion Zone Avoidance.

The MILP can be augmented by exclusion zone constraints following the approach of [41, 42]. As an example, consider a rectangular exclusion zone avoidance requirement given by $(\phi, \theta, \psi) \notin [-\phi_l, \phi_u] \times [-\theta_l, \theta_u] \times [-\psi_l, \psi_u]$. These zones restrict the available state space to a non-convex set. To handle such an exclusion zone, we augment our MILP with extra binary integer variables $\epsilon_{i,k} \in \{0, 1\}$ and constraints,

$$\begin{aligned} \phi_k &\leq \phi_l + M\epsilon_{1,k} \\ -\phi_k &\leq -\phi_u + M\epsilon_{2,k} \\ \theta_k &\leq \theta_l + M\epsilon_{3,k} \\ -\theta_k &\leq -\theta_u + M\epsilon_{4,k} \\ \psi_k &\leq \psi_l + M\epsilon_{5,k} \\ -\psi_k &\leq -\psi_u + M\epsilon_{6,k} \\ \sum_{i=1}^{6} \epsilon_{i,k} &\leq 5, \end{aligned} \tag{53}$$

where M is sufficiently large. The number of ϵ variables at each time step k is equal to the number of faces of the exclusion zone, with each $\epsilon_k = 1$ if the state lies “inside” the corresponding face and $\epsilon_k = 0$ otherwise. The final inequality ensures that the state remains outside of the exclusion zone, as the constraint is violated if and only if the state is “inside” of every face simultaneously, i.e., within the exclusion zone.

For the example presented in Figures 13 and 14, we included two waypoints and two exclusion zones. While in theory there is no limit to the number of exclusion zones that can be treated in this fashion, in practice we limited our simulations to two such zones to keep the computational burden as low as possible. The exclusion zones were centered at (-20°, -20°, 20°) and (-8°, -8°, 8°), with side length 4. The time steps were set at 3 seconds, except when the trajectory drew close to the waypoint set, then the time steps were reduced to 0.75 seconds for finer control accuracy. The waypoints were located at (0°, 0°, 0°) and (-40°, -40°, 40°) and were tracked one at a time in turn.

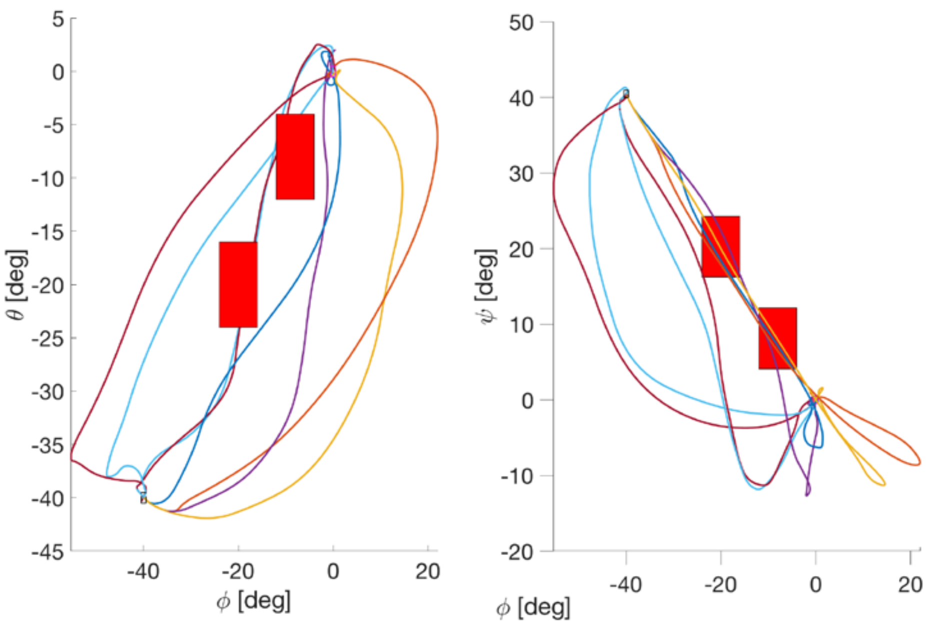

Figure 13. Two Obstacle Avoidance while Tracking Two Waypoints in turn with the MPC Solver

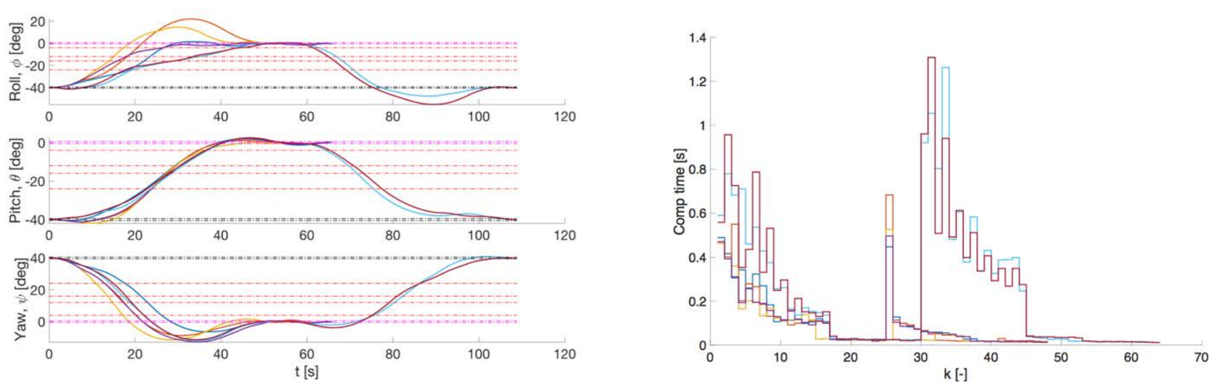

(a) **(b)**

Figure 14. Evolution of State and Computation Time at Each Time Step
(a) Evolution of the Individual Roll-Pitch-Yaw States with Time; (b) Computation time for each Time Step

We estimated a lower bound for the minimum time horizon, then solve the MILP once; if the solution was such that $\delta_N = 1$, then the horizon was extended and the MILP solved again. Once the MILP returned a solution with $\delta_N = 0$, then the control was optimal and the first move was applied, then the loop was closed by applying the MPC solver. All computations were carried out on a MacBook laptop with a 2.5 GHz processor and 16 GB of memory using Matlab's *intlinprog* command to solve the MILP; with this setup, the two waypoints were successfully tracked in turn while avoiding the exclusion zones, seen in Figures 13 and 14a, and even the worst-case computation times, seen in Figure 14b, were under 1.5 seconds for any given time step.

5. CONCLUSIONS

An invariance-based waypoint following control method has been developed to generate safe relative motion trajectories between NMTs. The results demonstrate that the method is effective in generating fuel-efficient trajectories that satisfy control and exclusion zone constraints. An NMPC controller has been developed for spacecraft attitude control and results showed that the developed control scheme is capable of executing rest-to-rest attitude maneuvers while enforcing constraints. The parameter governor methods to attain and maintain formations of spacecraft have been extended. The theoretical results provide guarantees that, under suitable assumptions, the parameter governor, which allows for non-linear dynamics and multiple parameters per vehicle in formation, can be applied to attain formations containing an arbitrary number of vehicles. The simulation results demonstrate implementation to attain a formation of three spacecraft and illustrated that a combined TSG/SSG can provide better performance than either the TSG or SSG alone in certain cases. Finally, in the context of a specific mission of a satellite inspection, the Local Gradient control technique has been analyzed to demonstrate robustness to initial condition and bounded disturbances, as well as to assess the effect of parameter values and control switching criteria on control usage and information collection.

REFERENCES

[1] Grune, L., and Pannek, J., **Nonlinear Model Predictive Control**, Springer, New York, NY, 2011.

[2] Mayne, D.Q., “Model Predictive Control: Recent developments and future promise,” *Automatica*, vol **50**, no. 12, 2014, pp. 2967–2986.

[3] Breger, L., How, J., and Richards, A., “Model predictive control of spacecraft formations with sensing noise," *Proceedings of the American Control Conference,* Portland, OR, vol **4**, 2005, pp. 2385-2390.

[4] Manikonda, V., Arambel, P. O., Gopinathan, M., Mehra, R. K., and Hadaegh, F., “A model predictive control-based approach for spacecraft formation keeping and attitude control," *Proceedings of the American Control Conference*, San Diego, CA, vol **6**, 1999, pp. 4258-4262.

[5] Morgan, D., Chung, S., and Hadaegh, F. Y., “Model predictive control of swarms of spacecraft using sequential convex programming," *Journal of Guidance, Control, and Dynamics*, vol **37**, no. 6, 1998, pp. 1725-1740.

[6] Petersen, C., Leve, F., and Kolmanovsky, I., "Model Predictive Control of an Underactuated Spacecraft with Two Reaction Wheels," *Journal of Guidance, Control, and Dynamics*, vol **40**, no. 2, 2017, pp. 320-332.

[7] Sauter, L. and Palmer, P., “Analytic model predictive controller for collision-free relative motion reconfiguration," *Journal of Guidance, Control, and Dynamics*, vol **35**, no. 4, 2012, pp. 1069-1079.

[8] Breger, L. and How, J. P., “Gauss’s variational equation-based dynamics and control for formation flying spacecraft,” *Journal of Guidance, Control, and Dynamics,* vol **30**, no. 2, 2007, pp. 437–448.

[9] Garone, E., Di Cairano, S., and Kolmanovsky, I., “Reference and command governors for systems with constraints: A survey on theory and applications,” *Automatica,* vol **75**, 2017, pp. 306–328.

[10] Kolmanovsky, I. V., and Sun, J., “Parameter Governors for Discrete-Time Nonlinear Systems with Pointwise-in-Time State and Control Constraints,” *Automatica,* vol **42**, no. 5, 2006, pp. 841–848.

[11] Bacconi, F., Mosca, E., and Casavola, A., “Hybrid constrained formation flying control of microsatellites," *Institution of Engineering and Technology Control Theory & Applications*, vol **1**, no. 2, 2007, pp. 513-521.

[12] Frey, G., Petersen, C., Leve, F., Garone, E., Kolmanovsky, I., and Girard, A., “Time Shift Governor for Coordinated Control of Two Spacecraft Formations,” *Proceedings of the 10th IFAC Symposium on Nonlinear Control Systems*, IFAC, Monterey, CA, 2016, pp. 302-307.

[13] Frey, G., Petersen, C., Leve, F., Garone, E., Kolmanovsky, I., and Girard, A., "Parameter Governors for Coordinated Control of n-Spacecraft Formations," *Journal of Guidance,Control, and Dynamics,* vol **40**, no. 11, 2017*,* pp. 3020-3025.

[14] Petersen, C., and Kolmanovsky, I., "Coupled Translation and Rotation Dynamics for Precise Rendezvous and Docking with Periodic Reference Governor Control Scheme," *Proceedings of Space Flight Mechanics Meeting*, 26th AAS/AIAA, Napa, CA, 2016.

[15] Blanchini, F., and Miani, S., **Set-Theoretic Methods in Control**, Birkhauser, Basel, Switzerland, 2008.

[16] Weiss, A., Leve, F., Baldwin, M., Forbes, J., and Kolmanovsky, I.V., "Spacecraft constrained attitude control using positively invariant constraint admissible sets on SO(3)$\times R^3$," *Proceedings of 2014 American Control Conference*, Portland, OR, 2014, pp. 4955-4960.

[17] Weiss, A., Petersen, C., Baldwin, M., Erwin, R.S., and Kolmanovsky, I.V., "Safe positively invariant sets for spacecraft obstacle avoidance," *Journal of Guidance, Control, and Dynamics*, vol **38**, no. 4, 2015, pp. 720-732.

[18] "Program Aims to Facilitate Robotic Servicing of Geosynchronous Satellites," URL: http://www.darpa.mil/news-events/2016-03-25, Accessed June 21, 2018.

[19] "Geosynchronous Space Situational Awareness Program (GSSAP)," URL: http://www.afspc.af.mil/About-Us/Fact Sheets/Article/730802/geosynchronous-space-situational-awareness-program-gssap, Accessed June 21, 2018.

[20] Fredrickson, S. E., Abbott, L. W., Duran, S., Jochim, J. D., Studak, J. W., Wagenknecht, J. D., and Williams, N. M., "Mini AERCam: development of a free-flying nanosatellite inspection robot," *International Society for Optics and Photonics*, 2003, pp. 97–111.

[21] Jacobovits, A., and Vaneck, T., "AeroAstros Escort–a microsatellite for on-orbit inspection of space assets," *Proceedings of the 17th Annual Conference on Small Satellites*, AIAA/USU, Logan, UT, 2003.

[22] Kim, S. C., Shepperd, S.W., Norris, H. L., Goldberg, H. R., and Wallace, M. S., "Mission design and trajectory analysis for inspection of a host spacecraft by a microsatellite," *Proceedings of 2007 IEEE Aerospace Conference*, Big Sky, MT, 2007, pp. 1–23.

[23] Clohessy, W. H., and Wiltshire, R. S., "Terminal Guidance System for Satellite Rendezvous," *Journal of the Aerospace Sciences,* vol **27**, no. 9, 1960, pp. 653–658.

[24] Frey, G., Petersen, C., Leve, F, Kolmanovsky, I., and Girard, A., "Constrained spacecraft relative motion planning exploiting periodic natural motion trajectories and invariance," *Journal of Guidance, Control, and Dynamics*, vol **40**, no. 12, 2017, pp. 3100-3115.

[25] Frey, G., Petersen, C., Leve, F., Kolmanovsky, I., and Girard, A., "Incorporating periodic and non-periodic natural motion trajectories into constrained invariance-based spacecraft relative motion planning," *Proceedings of 1st IEEE Conference on Control Technology and Applications*, Kohala Coast, HI, 2017, pp. 1811-1816.

[26] Even, S., **Graph Algorithms**, Cambridge University Press, Cambridge, UK, 2011, p. 15.

[27] Chang, Y.-h., Hyun, B., and Girard, A. R., “Path planning for information collection tasks using bond energy algorithm,” *Proceedings of American Control Conference*, Montreal, Canada, 2012, pp. 703–708.

[28] Frey, G., “Advances in Constrained Spacecraft Relative Motion Planning,” *Ph.D. Dissertation,* The University of Michigan, 2018.

[29] Casavola, A., Garone, E., and Tedesco, F., “Scalability and performance improvement of distributed sequential command governor strategies via graph colorability theory,” *IFAC Proceedings Volumes,* vol **47**, no. 3, 2014, pp. 9400–9405.

[30] Casavola, A., Garone, E., and Tedesco, F., “A distributed command governor based on graph colorability theory,” *International Journal of Robust and Nonlinear Control*, vol **28**, no. 8, 2018, pp. 3056–3072.

[31] Frey, G., Petersen, C., Leve, F., Girard, A., and Kolmanovsky, I., "Safe Relative Motion Trajectory Planning for Satellite Inspection," *Proceedings of Space Flight Mechanics Meeting*, AAS/AIAA, San Antonio, TX, 2017.

[32] Vallado, D. A., **Fundamentals of Astrodynamics and Applications**, Microcosm Press, Portland, OR, 2013, p. 846.

[33] Klesh, A. T., Kabamba, P. T., and Girard, A. R., “Optimal path planning for uncertain exploration,” *Proceedings of American Control Conference,* St. Louis, MO, 2009, pp. 2421–2426.

[34] Klesh, A. T., Kabamba, P. T., and Girard, A. R., “Path planning for cooperative time-optimal information collection,” *Proceedings of American Control Conference*, Seattle, WA, 2008, pp. 1991–1996.

[35] Shannon, C., “A Mathematical Theory of Communication,” *The Bell System Technical Journal*, vol **27**, 1948, pp. 379–423.

[36] Karpenko, M. and Ross, I.M., “Flight Implementation of Shortest-Time Maneuvers for Imaging Satellites,” *Journal of Guidance, Control, and Dynamics*, vol **37**, no. 4, 2014, pp. 1069-1079.

[37] Rawlings, J.B. and Mayne, D.Q., **Model Predictive Control: Theory and Design**, Nob Hill Publishing, Madison, WI, 2009.

[38] Borrelli, F., and Bemporad, A., and Morari, M., **Predictive Control for Linear and Hybrid Systems**, Cambridge University Press, Cambridge, UK, 2017.

[39] Floudas, C.A., **Nonlinear and Mixed-Integer Optimization – Fundamentals and Applications**, Oxford University Press, Oxford, UK, 1995.

[40] Sutherland, R, and Kolmanovsky, I., and Girard, A., “Attitude Control of a 2U Cubesat by Magnetic and Air Drag Torques,” IEEE Transactions on Control Systems Technology, 2018, pp. 1-13.

[41] Richards, A., and Schouwenaars, T., and How, J.P., and Feron, E., "Spacecraft Trajectory Planning with Avoidance Constraints Using Mixed-Integer Linear Programming," *Journal of Guidance, Control, and Dynamics*, vol **25**, no. 4, 2002, pp. 755-764.

[42] Zhang, L., and Zhou, Z., and Zhang, F., "Mixed Integer Linear Programming for UAV Trajectory Planning Problem," *Applied Mechanics and Materials*, vol **541-542**, 2014, pp 1473-1477.

LIST OF SYMBOLS, ABBREVIATIONS, AND ACRONYMS

AFRL	Air Force Research Laboratory
DARPAs	Defense Advanced Research Projects Agency
LG	Local Gradient
LQR	Linear quadratic regulator
MILP	Mixed-Integer linear program
LVLH	Local-vertical/local- horizontal
MPC	Model predictive control
NMPC	Nonlinear model predictive control
NMT	Natural motion trajectory
OCP	Optimal Control Problem
QPP	Quadratic Programming Problem
PI	Principal Investigator
RSGS	Servicing of Geosynchronous Vehicles
TSG	Time shift governor
SSG	Scale shift governor

DISTRIBUTION LIST

DTIC/OCP 8725 John J. Kingman Rd, Suite 0944 Ft Belvoir, VA 22060-6218	1 cy
AFRL/RVIL Kirtland AFB, NM 87117-5776	1 cy
Official Record Copy AFRL/RVSV/Christopher Petersen	1 cy